NASA

Technical Memorandum 79549

(NASA-TM-79549) THE ANALYSIS OF TEMPORAL VARIATIONS IN REGIONAL MODELS OF THE SARGASSO SEA FROM GEOS-3 ALTIMETRY
Technical Memorandum, Jul. 1975 - Aug. 1976
(NASA) 58 p HC A04/MF A01 CSCL 08C G3/48

N78-27725
Unclas
25787

The Analysis Of Temporal Variations In Regional Models Of The Sargasso Sea From GEOS-3 Altimetry

R. S. Mather, R. Coleman, and B. Hirsch

May 1978

National Aeronautics and Space Administration

Goddard Space Flight Center
Greenbelt, Maryland 20771

TM 79549

THE ANALYSIS OF TEMPORAL VARIATIONS IN REGIONAL MODELS OF THE SARGASSO SEA FROM GEOS-3 ALTIMETRY

R.S. Mather*
Geodynamics Branch
Goddard Space Flight Center
Greenbelt, Md 20771

R. Coleman*
B. Hirsch*
Department of Earth and Planetary Sciences
Johns Hopkins University
Baltimore, Md 21218

May 1978

*On leave of absence from the University of New South Wales, Sydney, Australia.

Presented at the Second International Symposium
"The Use of Artificial Satellites for Geodesy and Geodynamics"
Lagonissi, Greece
May 29 to June 3 1978

GODDARD SPACE FLIGHT CENTER
Greenbelt, Maryland

CONTENTS

TABLES

ILLUSTRATIONS

THE ANALYSIS OF TEMPORAL VARIATIONS IN REGIONAL MODELS OF THE SARGASSO SEA FROM GEOS-3 ALTIMETRY

R. S. Mather*
R. Coleman*
B. Hirsch*

ABSTRACT

The dense coverage of short pulse mode GEOS-3 altimeter data in the western North Atlantic provides a basis for studying time variations in the sea surface heights in the Sargasso Sea. Two techniques are utilized in this study·

- the method of regional models; and
- the analysis of overlapping passes.

Monthly models of the Sargasso Sea are produced for the period July to November 1975 and from April to August 1976. The analysis of the heights of common 0.2° x 0.2° squares indicates a root mean square (rms) discrepancy of ±43 cm in values produced from different solutions. Approximately one quarter of this is due to the variation in geoid slope across 0.2° squares. The residual discrepancy is due to instabilities introduced by variable pass geometry, unmodelled ocean tides and meoscale variations in sea surface topography. Shortwave maxima and minima in the regional sea surface models are examined for correlations with surface and remote sensed infrared temperature data. On allowing for differences in the quantities being compared, an 88 percent correlation is obtained between the location of cyclonic eddies obtained from infrared imagery and reported by the National Weather Service, and sea surface height minima in the altimeter models. This figure drops to 59 percent in the case of correlations with maxima and minima of surface temperature fields.

The analysis of overlapping passes provides a better picture of instantaneous sea state through wavelengths greater than 30 km. The resolution obtained is significantly higher (±33 cm on average) through the areal representation is limited to 32 selected profiles. Correlation studies with cyclonic and anti-cyclonic ocean eddies from the NIMBUS 6 and GEOS I and II infrared imagery indicate satisfactory agreement being obtained with equivalent sea surface height features 98 percent of the time if time varying factors are allowed for. The spectral analysis of the overlapping

*On leave of absence from the University of New South Wales, Sydney, Australia.

passes shows once again the high relative precision of the GEOS-3 altimeter in the short pulse mode. The variability of the Sargasso Sea through wavelengths between 150 km and 5000 km is estimated at ±28 cm. On considering the magnitude of unmodelled orbital error this value is in reasonable agreement with oceanographic estimates and is compatible with the eddy kinetic energy of a wind driven circulation.

An approximate estimation technique shows that the quasi-stationary SST maintaining the Gulf Stream is present in the GEOS-3 data but cannot be estimated with confidence in the absence of an adequate geiodal model.

THE ANALYSIS OF TEMPORAL VARIATIONS IN REGIONAL MODELS OF THE SARGASSO SEA FROM GEOS-3 ALTIMETRY

1. THE DATA BASE

The GEOS-3 spacecraft, launched in April 1975, was used to acquire short pulse mode radar altimeter ranges in the form of discrete passes not exceeding 20 minutes in length, off the east coast of the United States. The relative precision of GEOS-3 altimeter data recorded in the Tasman and Coral Seas was found to be ±20 cm (Mather and Coleman 1977) though the values provided by Wallops Flight Center after pre-processing, are usually in error by up to 2 orders of magnitude greater than this value (Mather et al. 1977, p.30).

These earlier studies indicated that the intensive mode GEOS-3 altimeter data contained information on regional variations in the height of the sea surface (ζ) with wavelengths which were less than twice the maximum pass length (i.e., less than 9000 km) and with amplitudes which were greater than ±10 cm. It was also found that factors pertaining to either the sea state or else, the method of averaging used in the altimeter, may cause problems in the resolution of features of wavelengths much less than 30 km (Mather 1977, p.25).

The area covered by the dense network of GEOS-3 altimetry is shown in Figure 1. Table 1 sets out a summary of the data available in the 1977 GEOS-3 altimeter data bank at Goddard Space Flight Center. The data is catalogued on a monthly basis from April 1975 to August 1976. This data was selected in two different ways to study regional variations in ζ.

In the first, the intensive mode GEOS-3 altimetry was processed on a monthly regional basis using the intersection of passes to provide a framework of control for the adjustment of the sea surface model (Mather et al. 1977, pp. 37 et seq.). It was assessed that meaningful models of the sea surface could not be obtained unless the number of passes (n) approached 15 and the number of junction points were approximately 4n. It was decided on this basis, to restrict the study of time variations on a regional basis from monthly analyses, to the period July to November 1975, and April to August 1976. These studies are described in Section 2. Section 3 studies the correlations between such satellite-determined models of the sea surface and their variations against surface and remote-sensed temperature data and the location of eddies in the test area.

The second data base was prepared using the observation that GEOS-3 groundtracks approximately repeat themselves every 526 revolutions. This occurs after 37.18 days. Profiles of intensive mode GEOS-3 altimetry in the Sargasso Sea test area (Figure 1) which occur over the same groundtrack after a lapse of 526 revolutions or multiples thereof, were sorted into separate data sets. Thirty-two such sets of overlapping passes are available for analysis in the test area, and their groundtracks are shown in Figure 2.

Table 2 sets out detailed information on the 32 sets of overlapping passes which are used in the present study in the Sargasso Sea. Section 4 describes the techniques used in the study of sets of overlapping passes and the results obtained from the analysis of such data.

2. REGIONAL SEA SURFACE MODELLING

Early studies of intensive mode GEOS-3 altimetry in the Tasman and Coral Seas off eastern Australia (Mather et al. 1977; Mather 1977) indicated that passes of altimetry data provided to Principal Investigators were subject to orbital errors varying from ±2 m to in excess of ±10 m. Pairs of overlapping passes in this data bank were studied, these included a pair where one of the passes was subject to a radial error in excess of 700 m. The relative discrepancy could be reduced to ±61 cm of which 66 percent occurred with wavelengths equal to twice the length of the pass if the passes were fitted to each other (Mather and Coleman 1977, Tables 1 and 2, Row 1). The improved relative fit was obtained by applying a correction for tilt c and bias b per pass with lengths in excess of 10^3 km. In less extreme cases, the root mean square (rms) discrepancy after allowing for tilt and bias, is significantly smaller. A typical figure (Table 2) is ±30 cm over a 3000 km pass.

As such, it is possible to model the quasi-stationary sea surface height (ϕ,λ) at the point whose latitude is ϕ and longitude λ in terms of estimates $\zeta_{ij}\ (\phi,\lambda)$ from the j-th element of the i-th pass of GEOS-3 altimetry using the relation

$$\zeta = \zeta_{ij} + b_i + c_i\ (t_{ij} - t_{i1}) + \zeta_t + v_r \qquad (1)$$

on dropping the position identifier, ζ_t being the height of the combined Earth and ocean tide, t_{ij}, t_{i1} the times of the j-th and first elements in the i-th pass. v_r would represent all unmodelled effects including mesoscale variations in the dynamic sea surface topography (SST).

The estimates of ζ from values ζ_{ij} and $\zeta_{k\ell}$ on the i-th and k-th passes which intersect at P, give two equations of the form at (1), which on combination, give an observation equation of the form

$$v = \zeta_{ij} - \zeta_{k\ell} + (b_i - b_k) + c_i\ (t_{ij} - t_{i1}) - c_k\ (t_{k\ell} - t_{k1}) \qquad (2)$$

on assuming that the tidal signal can be treated as being included in either ζ or v.

The first stage in devising an impersonal and flexible system in regional sea surface modelling, is the definition of an event which is construed as a crossover (or junction point). The GEOS-3 altimeter has a finite footprint. Therefore one possibility is to treat a p° x p° square as a junction point. Table 3 sets out the residual statistics (i.e., the rms value of v in equation 2) obtained when adjusting the same block of data using different values of p. If

$$\sigma = \sum_{i=1}^{N} \left(v_i^2 \right)^{1/2} \qquad (3)$$

where N is the number of junction (crossover) points, the dominant contribution to σ is the slope of the sea surface if $p>0.2$, being almost 99 percent of σ for 1° x 1° junction points (Mather et al. 1977, p.40) as illustrated in Table 3.

The noise level of the GEOS-3 altimeter is assessed at ±20 cm on a relative basis. The value of σ should be kept as small as possible so that time variations on a regional basis can be recovered with an equivalent resolution. However, computer limitations and the finite footprint of the altimeter also limit the minimum value p can take. A good compromise is an 0.2° x 0.2° square. The geoid variations within such a square should not materially mask features in the sea surface with amplitudes greater than ±25 cm and wavelengths in excess of 40 km. Regional sea surface models obtained from solutions based on 0.2 degree squares as crossover "points" should be adequate for the location of eddies in the western Sargasso Sea which are expected to have exhibit sea surface height variations in excess of ±50 cm over extents as large as 10^2 km (e.g., Cheney and Richardson 1976).

The basic area in which GEOS-3 altimetry data was analysed for the generation of regional sea surface models is a 12° x 12° area shown in Figure 1. The ocean tides were treated as noise in the present series of computations as the inclusion of a current tidal model in a sample had a negligible effect on the heights of the sea surface as summarized in Table 4 and Figure 3.

Table 1 sets out all data used in this analysis (Rows 4 to 8 and 13 to 17) detailing the number of passes and junction points and values of σ obtained after adjustment. It has been noticed that the value of σ increases slightly as the volume of data increases. This is probably due to the fact that noisy records are not filtered out of the solutions. A second observation concerns the relatively larger values of σ for July, August and September 1975 (Table 1; Rows 5, 6 and 7). This cannot be attributed to orbital error. Possible causes for this may be time tag errors which occur from time to time in the 1977 GEOS-3 altimetry data bank. The authors are not aware of any reason to believe that this reflects an increasingly noisy sea for the period.

The monthly sea surface models so obtained are

- insensitive to absolute datum, being based on a set of observation equations which are differential in nature (Equation 2); and
- subject to slight arbitrary variations in Earth space orientation which is a function of the location of the junction points over the area (Figures 4 to 13). It was therefore decided to provide an absolute datum to the 10 monthly models by making a three parameter fit to the best available satellite gravity field model GEM 9 (Lerch et al. 1977).

The orientation was effected by using observation equations of the form

$$v = \zeta - \zeta_{GEM\ 9} + a_0 + a_1\ (\phi - \phi_0) + a_2\ (\lambda - \lambda_0) \qquad (4)$$

over the test area which was approximately 1200 km long, ϕ_0, λ_0 being co-ordinates of the southwest corner of the region studied. The corrections obtained are listed in Table 5. The variation in the overall tilt between different sea surface models to GEM 9 is less than 10 cm per 10^2 km. This is a measure of the stability obtained internally in each monthly solution and is of adequate resolution for studies of variations in sea surface topography which have magnitudes in excess of 20 cm in relation to the surrounding oceans. It must be emphasized that the data generated from the ten monthly solutions can only be used for the study of variations in the sea surface topography and not the quasi-stationary SST for which a geoid of adequate precision is required. While the discrepancy between the heights of the sea surface from different monthly solutions disagree by less than ±40 cm on the average in areas covered by altimetry, the disagreement with the best available geoid (Marsh and Chang, 1978) is considerable, the discrepancies being correlated with distance from the east coast of North America, as illustrated in Figure 15. This is probably due to the decreasing density of gravity data of adequate quality as a function of position in computations of the gravimetric geoid.

The contours shown in Figures 4 to 13 are estimated heights of the average sea surface for the month relative to the mean sea surface for the epoch (July 1975 to August 1976) with wavelengths greater than 200 km and do not reflect the quasi-stationary sea surface topography in the region. The plots represent wavelengths greater than 200 km, but enhanced by additional data in the vicinity of eddies. Thus the contours of the quasi-stationary component of the Gulf Stream to the west of the test area, have been filtered out of the solution. Attempts to recover the quasi-stationary component of the Gulf Stream are described in the Appendix.

The values of σ obtained for the solutions, except in the three cases mentioned above, are only marginally greater than the expected variation of the geoid over a 0.2° square. However, the contours in Figures 4 to 13 are reliable only in the vicinity of groundtracks shown on the Figures. The precision of contours is significantly worse than $\pm\sigma$ in Table 1 at locations more than 50 km away from a groundtrack. Contours shown in broken lines should be treated as suspect with errors being as large as ±1 m.

The models shown in the above figures do not exclude the ocean tides. Earlier studies in the Tasman and Coral Seas (Mather et al. 1977, p.40) showed that the Hendershott tidal model provided with the Wallops tapes did not materially affect the statistics of regional solutions. As it is widely held that the tidal models in the Sargasso Sea are of better quality than those in the Tasman and Coral Seas, it was decided to test whether the application of the ocean tide model would improve the values of σ obtained. This was not found to be the case (see Table 4). The application of the Hendershott tidal model as provided by Wallops Flight Center for a test period of one month which has the most data (October 1975) was found to produce no change in the residuals σ after adjustment. The average value of the heights of the 243 crossover points changed by 0.03 m. The change in values of ζ_s is highly

correlated with position, as shown in Figure 3. However, the magnitude of the effect was considered too small to warrant consideration in the present study.

The ten regional monthly solutions so obtained were examined against mean monthly measurements of surface temperature in the area and against tracks of eddies obtained from satellite remote sensing, as described in the next section.

3. CORRELATIONS OF REGIONAL MONTHLY MODELS OF DYNAMIC SEA SURFACE TOPOGRAPHY VARIATIONS WITH SURFACE OCEAN DATA

The Sargasso Sea lies to the east of the Gulf Stream. It is one of the best surveyed oceans in the world for surface temperature fields. The motion of the major eddies and the location of both the edge of the slope water and the Gulf Stream are monitored on a monthly basis and a monthly record published by the US National Weather Service (NOAA 1975; NOAA 1976). The following dominant features reported in this publication:

- the location of eddies; and
- the clearly defined maximum and minimum mean monthly temperatures for 1° x 1° squares

are also located in Figures 4 to 13.

Most of the comparisons occur in deep oceans and the significance of the results, illustrated in Figures 4 to 13 and listed in Table 6 can be interpreted as follows. Assuming the existence of a layer of no motion at great depth H ($\doteq$ 2000 m) in the region at which isobaric and level surfaces coincide, the constant pressure P at depth (h = H) is given by

$$P = \left[\int_H^0 g\,\rho_w\,dz\right]_{\text{Ocean}} + \left[\int_0^{h_a} g\,\rho_a\,dz\right]_{\text{Atmosphere}} = \text{Constant} \qquad (5)$$

where g is observed gravity, ρ_w the density of sea water and ρ_a the atmospheric density at the element of height dz for a given location, the integration being along the local vertical. The variations in ρ_w, ρ_a cause anomalies dh in the height of the standard column of water above the level of no motion. These can be related to temperature anomalies dT at the pressure increment dp corresponding to dz, in terms of the relation

$$dh = \frac{1}{g}\left[\int_P^{P_o} \frac{\partial \alpha}{\partial T}\,dT\,dp - \frac{1}{\rho_w}\,dp_a\right] + o\{f\,dh\} \qquad (6)$$

where α is the specific volume of sea water and dp_a the atmospheric pressure anomaly from the standard atmospheric model at the air/sea interface where the pressure is P_o.

The density of sea water ρ_w varies from 1.022 in the surface layers of equatorial oceans to 1.028 in deep oceans (Monin et al. 1974, p.36). Expressed in terms of α, these variations as a function of temperature can be expressed by a relation of the form

$$\alpha_w = (\alpha - 1) \times 10^{-4} = a_1 + a_2 \log_e T \qquad (7)$$

The use of the table in (Dietrich 1963, p.44) in evaluating a_1 and a_2 in equation 7 gives

$$a_1 = -5.18 \times 10^{-5} \quad ; a_2 = 8.72 \times 10^{-6} \qquad (8)$$

for T in °K and ρ_w in g cm^{-3}, in the range 0°C to 40°C with a correlation coefficient of 0.9. Thus

$$\frac{\partial \alpha}{\partial T} = 10^4 \frac{a}{T^2} \text{ cm}^3 \text{ g}^{-1} (^\circ\text{K})^{-1} \qquad (9)$$

Table 7 sets out values of $\partial\alpha/\partial T$ which conform with a model defined by equations 7 and 8. It also provides a simplified, even simplistic estimate of the sea surface height anomaly which can be expected from a typical Gulf Stream eddy. For example, the cyclonic eddy reported by Cheney and Richardson (1967, p.145) is equivalent to changes in SST of between -60 cm and -152 cm, assuming a level of no motion at 1000 m deep. Temperature anomalies which average 1°C over 2000 m are equivalent to a SST anomaly of approximately 60 cm. Surface temperature measurements do not appear to be representative of the entire oceans especially if representative of an eddy-type structure (ibid). In the case of such structures, temperatures from the deeper layers have a greater influence on local SST maxima and minima than an estimate of the surface temperature which could be deceptively near normal.

Consequently, correlations between surface temperature measurements and local maxima and minima in the shape of the sea surface should not be expected in all cases.

An examination of Figures 4 to 13 also show that there is not always an exact correlation between the location of cyclonic eddies in the Sargasso Sea and lows in the surface temperature means, on the one hand, and SST lows on the other. There are two possible reasons for this

- Gulf Stream rings have been observed to move at irregular rates of up to 8 km per day (Richardson et al. 1973, p.297).
- The surface temperature is no indicator of the existence of a cold cyclonic eddy (Cheney and Richardson 1976, p.145)
- The Gulf Stream ring locations are given at the end of each month, while the altimetry-determined highs are based on data collected at various times over a month and therefore reflect average conditions for the month.

Table 6 summarises the extent of correlation between

a) cyclonic rings shown in (NOAA 1975, NOAA 1976) and lows in the GEOS-3 altimeter models of the sea surface shape, and
b) highs in both the monthly sea surface temperature means (ibid) as well as in the altimeter model.

None of the comparisons made between cyclonic eddies and sea surface lows can be classified as being unsatisfactory, given the differences between the two types of information compared. The correlation between the altimeter sea surface model and mean sea surface temperatures is less impressive. Sixteen percent of the comparisons obtained were not positive. This is not unexpected as surface temperature anomalies are not necessarily an indicator of any equivalent SST anomaly.

In view of this evidence, it can be concluded that regional sea surface modelling has achieved a precision of ±40 cm and provides a reliable basis for the study of eddies which cause larger variations in sea surface heights.

These figures only apply in the immediate vicinity of groundtracks. The precision falls off rapidly with distance from the nearest groundtracks. Unless the geometry of the passes is grossly irregular (e.g., Figures 4 or 9), it appears that the precision of sea surface models is seldom worse than ±1 m.

However, there are too many exceptions to claim 100% reliability at these levels. So far, no data has been excluded. However, departures of the monthly regional sea surface height from the mean of ten solutions are strongly correlated with position, as illustrated in Figure 16. There is a tendency towards weak determinations at the peripheries of the region being studied. There is extra strength in this index of variability at the edges abutting the Gulf Stream.

The contours shown in Figures 4 to 13 specifically exclude the quasi-stationary component of the SST. The possibility of recovering this part of the spectrum of SST at the present time is discussed in the Appendix. The contours shown in these figures are based on data on a one degree grid and thereby reflect wavelengths greater than 200 km. Additional data was plotted at 20 km intervals to enhance local features in areas where infrared imagery reported the existence of cyclonic eddies.

The significance of the contours referred to above is hard to assess. The solution statistics do not indicate confidence in features with wavelengths much longer than 200 km unless they have amplitudes in excess of 40 cm. This restricts any analysis to the region in the vicinity of the Gulf Stream. However, the results in this peripheral area may be flawed by geometrical uncertainties. These should not be treated as limitations of the regional altimetric technique used in this study. A much improved solution can be obtained under the following circumstances.

i) The region is covered with an adequate network of passes.
ii) A reasonable tidal model is available for the area.

These limitations can be avoided in the processing of SEASAT-A data. The present study should be treated as preliminary. The possibility still exists that the results can be refined by a factor of 60% by re-processing the data with an accurate tidal model. A project for the recovery of the tidal signal from the GEOS-3 altimetry is currently underway.

A 25% improvement in the resolution can be obtained by restricting the study to those limited number of cases where the groundtracks satisfy the overlap condition.

4. THE ANALYSIS OF OVERLAPPING PASSES IN THE SARGASSO SEA

The orbital period of the GEOS-3 spacecraft is approximately 101.79 minutes. The condition for a repeated groundtrack after n revolutions is

$$\sum_{i=1}^{n} \left[\dot{\Omega}_i \, t_i - \omega_i \, t_i \right] = 0 \qquad (10)$$

on suppressing multiples of 2π in the second term, ω_i being the angular velocity of rotation of the Earth during the i-th revolution of GEOS-3 which is completed in time t_i, $\dot{\Omega}_i$ being the instantaneous rate of precession of the orbital node. This condition is nearly satisfied every 526 revolutions, the observed drifts ($\delta\lambda$) in longitude being set out in Figure 16. There is no simple pattern of overlaps in the Sargasso Sea test area due to the irregular manner in which data was collected. Nevertheless, a dense network of overlapping passes has been established in the western North Atlantic. Using the multiple of 526 revolutions as a criterion, 32 sets of from 5 to 9 overlapping passes were identified in the Sargasso Sea as illustrated in Figure 2.

Consider the case of the j-th element of the i-th pass and the ℓ-th element of the k-th pass which have identical latitudes, the i-th and k-th passes satisfying the overlap condition. The observed sea surface heights ζ_{ij} on the i-th pass and $\zeta_{k\ell}$ on the k-th pass can be used to set up observation equations of the form

$$\zeta_{ij} - \zeta_{k\ell} + (b_i - b_k) + c_i \, (t_{ij} - t_{il}) - c_k \, (t_{k\ell} - t_{kl}) + (\zeta_{tij} - \zeta_{tk\ell}) + \delta\lambda \, \frac{\partial N}{\partial \lambda} = v_s \qquad (11)$$

where (b_i, b_k) and (c_i, c_k) are corrections for bias and tilt to the i-th and k-th passes on account of orbit integration errors, $(\zeta_{tij}, \zeta_{tk\ell})$ are the tidal heights at the location at the instant of data acquisition $(t_{ij}, t_{k\ell})$, (t_{il}, t_{kl}) being the times corresponding to the initial instant of data acquisition per pass. The last term on the left in equation 11 allows for the slope of the geoid due to any possible longitudinal displacement $\delta\lambda$ between the pair of overlapping passes (Figure 16).

Table 2 sets out details of the 219 passes which make up the 32 overlapping sets shown in Figure 2. Passes where $\delta\lambda$ exceeded 35 km were excluded from this study.

The most striking feature of the results in Table 2 is the internal precision of the GEOS-3 altimetry reflected in the values of the root mean square discrepancy σ_m obtained by comparing each profile with the mean of the set after using equation 11 in the case where the mean profile replaces the k-th pass. The analysis of the values of σ_m in Table 2 as a function of length (Figure 17) shows some correlation with pass length to 4000 km. The data used in the construction of this figure has not been filtered in any way. The complexity of the Sargasso Sea test area makes it hard to draw simple conclusions.

Table 8 summarises the spectral analysis of the discrepancies between each pass and the average of the set for the largest of the sets (No. 8 in Table 2) containing 9 overlapping passes. The harmonic coefficients determined (A_1, B_i, where i is the integral number of complete wavelengths in the length ℓ over which comparisons are made) were given by the relations

$$\begin{bmatrix} A_1 \\ B_i \end{bmatrix} = \frac{2}{\ell} \int_0^{\ell} v_s \begin{bmatrix} \sin \\ \cos \end{bmatrix} \frac{2\pi s}{\ell} \, 1 \, ds \qquad (12)$$

where ds is the sampling interval, the residual v_s defined by equation 11 being at a distance s from the commencement of comparisons.

The significance of the amplitudes (A_1, B_i) so obtained is assessed by comparison against a spectrum of white noise (Mather 1977, p.17). If the rms residual of comparison is σ_m, the percentage contribution per frequency (E) to the white noise spectrum is given by

$$E = \frac{100}{N} \qquad (13)$$

where N is the number of frequencies between 1 and Nyquist limit imposed largely by the altimeter footprint ($\ell/10$).

The percentage strength of signal 0 obtained from equation 12 is defined by

$$0 = \frac{A^2 + B^2}{2\sigma_m^2} \qquad (14)$$

Table 9 sets out the results for all 32 sets of passes as an average per set. The root mean square (rms) residuals obtained in this area are somewhat larger than those obtained in the study of the Tasman and Coral Seas (Mather 1977, pp.24 and 25), averaging ±33 cm instead of ±20 cm obtained when each profile is fitted to the mean of the set of profiles (Coleman and Mather 1978).

Tables 8 and 9 are self-explanatory.* Significant strengths of signal (i.e., O/E>3) are obtained for several wavelengths in excess of 150 km. The average square of the strength of signal for wavelengths between 150 and 5000 is 784 cm^2 This is not unlike values quoted by oceanographers for the magnitude of seasonal variations and is compatible with variations in the SST arising from wind driven circulation.

The next stage in the processing of sets of overlapping passes is the analysis of the data for the tidal signal on a regional basis. In the interim, attempts have been made to study correlations between remote sensed temperature data and the variations in the sea surface heights as a function of position and time. These are reported in the Appendix (Sec. 8.2).

The analysis of overlapping passes provides the most accurate data for the study of regional variations in the dynamic sea surface topography. The limitations of coverage are offset by the 50 percent gain in precision over the regional solution method.

*Frequencies were grouped in "bins" according to wavelength (WL) to simplify the presentation of results.

5. CONCLUSIONS

There is no doubt that the GEOS-3 altimeter data in the short pulse mode is of sufficient precision for oceanographic studies. The main problem in regional studies remains the orbital uncertainty. These can be reduced to ±40 cm in the radial component if any claims to global relevance are sacrificed. This improves the resolution from ±1½ m globally (Mather et al. 1978) to ±40 cm on a regional basis if bad records are appropriately filtered, and if the geometry of passes is adequate (e.g., Figures 6-8). The technique of overlapping passes has a higher resolution (±33 cm on average).

The stability of the solutions is enhanced if very short passes are not subject to corrections for tilt (equation (1)). The internal statistics of solutions (in this case an average rms of ±25 cm) is almost a factor of 3 more optimistic than the estimated precision obtained from the intercomparison of solutions (±43 cm).

There is considerable confidence in recovering short wave features in sea surface shape which have dimensions between 30 and 100 km and amplitudes in excess of ±50 cm. Except in the case of solutions in 1975 where for some unaccountable reason, the solution statistics were significantly inferior (Table 1), there are variables in the sea surface with amplitudes in excess of 50 cm and dimensions in excess of 400 km (one third that of the region studied) which show up in this study. It can be concluded that the variations in SST with time in areas away from fast moving currents like the Gulf Stream are unlikely to exceed ±30 cm. This figure is confirmed by the spectral analysis of overlapping passes in the region.

This, in turn, indicates the necessity for the significant concentration of effort in generating force field models for the integration of orbits with radial errors much less than ±5 cm. There is little doubt that GEOS-3 data is of adequate resolution to study eddies. There are also grounds for cautious optimism that the data can be used to recover some of the dominant long wave characteristics of the quasi-stationary SST (ibid). Progress in other areas is likely to be slow in forthcoming till the gravity field models have been improved by at least an order of magnitude (hopefully, to 3 parts in 10^{-9}). This goal has to be achieved before further progress can be made in studying intermediate wavelengths of SST, both the quasi-stationary and time varying components.

Stringent criteria have to be enforced to exclude the 1% of noisy data encountered in the processing of GEOS-3 data. There is no real difficulty in identifying the faulty records.

Neither of the methods described has the potential to provide information on time variations in sea level which are constant over the entire area. Each method provides insight into certain portions of the spectrum of SST. The regional method cannot resolve features with periods shorter than a month (in the case of GEOS-3) while the higher-resolution technique of overlapping passes is restricted to selected groundtracks and variations with periods greater than a month. All information in the time varying part of the spectrum of SST with wavelengths greater than twice the dimension of the region studied are also lost.

The terms in the quasi-stationary part of the spectrum can only be recovered if an adequate gravity field model were available. The approximate estimating technique used in the Appendix shows that the large SST gradients maintaining the Gulf Stream are present in the GEOS-3 altimeter data. They are not recoverable with confidence at the present time.

6. ACKNOWLEDGMENTS

This project is supported by NASA Grant NSG 5225 and the Australian Research Grants Committee.

The first author worked on this project while holding Senior Resident Research Associateship of the US National Academy of Sciences at Goddard Space Flight Center while on leave of absence from the University of New South Wales.

The second author is supported by a Fulbright Travel Grant and Post-Graduate Award from the Government of Australia's Department of Education.

7. REFERENCES

Cheney, R.E. & Richardson, P.L., 1976. Observed Decay of a Cyclonic Gulf Stream Ring, Deep Sea Res., 23, 143-155.

Coleman R. & Mather, R.S., 1978. On the Determination of Time Varying Features in the Sea Surface Topography Using GEOS-3 Altimetry. EOS, 59 (4), 259.

Dietrich, G., 1963. General Oceanography - An Introduction. Wiley, New York.

Leitao, C.D., Huang, N.E. and Parra. E.G., 1977. Ocean Current Surface Measurement using Dynamic Elevations Obtained by the GEOS-3 Altimeter. Proc. Symp. Satellite Applications to Marine Technology, New Orleans, November 15-17, 1977. American Institute of Aeronautics & Astronautics, New York, 43-49.

Lerch, F.J., Klosko, S.M., Laubscher, R.E. and Wagner C.A., 1977. Gravity Model Improvement Using GEOS-3 (GEM 9 & 10). NASA/GSFC Rep. X-921-77-246, Goddard Space Flight Center, Greenbelt, Md., 121 pp.

Marsh, J.G. and Chang, E.S., 1978. Five Minute Detailed Gravimetric Geoid in the North Western Atlantic Ocean. Marine Geodesy, 1 (3) (In Press).

Mather, R.S., 1968. The Free Air Geoid for Australia. Geophys. J.R. Astr. Soc., 16, 515-530.

Mather, R.S., 1977. The Analysis of GEOS-3 Altimeter Data in the Tasman and Coral Seas. NASA Tech. Memorandum 78032, Goddard Space Flight Center, Greenbelt, Md., 32 pp.

Mather, R.S. and Coleman, R., 1977. The Role of Geodetic Techniques in Remote Sensing the Surface Dynamics of the Oceans. (In) Napolitano, L.G. (ed.). Using Space Today and Tomorrow. (Bergamon, Oxford) (In Press).

Mather, R.S., Coleman, R., Rizos, C. and Hirsch, B., 1977a. A Preliminary Analysis of GEOS-3 Altimeter Data in the Tasman and Coral Seas. International Symposium on Satellite Geodesy, Budapest, 28 June to 1 July 1977. Unisurv G, 26, 27-46.

Mather, R.S., Lerch, F.J., Rizos, C., Masters, E.G. and Hirsch, B., 1978. Determination of some dominant parameters of the dynamic sea surface topography from GEOS-3 Altimetry. NASA Tech. Memorandum 79558, Goddard Space Flight Center, Greenbelt, Md., 39 pp.

Monin, A.S., Kamenkovich, V.M. and Kort, V.G., 1974. Variability of the Oceans. Wiley, New York.

NOAA 1975. Gulfstream, 1 (1-12), US National Weather Service, Washington, D.C.

NOAA 1976. Gulfstream, 2 (1-120), Loc. cit. supra.

Richardson, P.L. Strong, A.E. and Knauss, J.A., 1973. Gulf Stream Eddies Recent Observations in the Western Sargasso Sea. J. Phys. Oceanography, 3, 297-301. May 1, 1978.

8. APPENDIX

8.1 The Quasi-Stationary Component of the Sea Surface Topography in the Vicinity of the Gulf Stream

The velocities reported in the vicinity of the Gulf Stream in the western part of the Sargasso Sea test area are greater than 10^2 cm s^{-1}. The sea surface topography gradient needed to maintain such a current should be about 1.5 x 10^2 cm per 10^2 km orthogonal to the mean direction of flow (Figure 1). This information can only be obtained from the GEOS-3 altimetry, processed in the form of regional models, as discussed in Section 2, if the sea surface heights were referred to an error free geoid. As seen from Figure 14, the discrepancies between the sea surface models from altimetry, after orientation to GEM 9 (Table 5), are systematically discrepant with the best available gravimetric geoid in the region (Figure 14). These discrepancies can be attributed to the following factors

i) Differences between the gravimetric geoid and the satellite determined gravity field model.
ii) The quasi-stationary component of the sea surface topography (SST).

For example, if it were assumed that the GEM 9 gravity field model were free from error, the differences at i) are due entirely to errors in the gravimetric geoid due to the variable quality and distribution of surface gravity data currently available for such computations in this region. As the gravimetric geoid is computed from a fixed gravity data bank using quadratures techniques, the resulting errors in the geoid are slowly varying functions of position (e.g., see Mather 1968). As the pattern of discrepancies is a function of distance from the east coast of North America (Figure 14), it is possible to make a very approximate estimate of the quasi-stationary SST from the pattern of contours in Figure 14.

On assuming that the gravimetric geoid error N has a structure

$$e_N = N_o + \frac{\partial N}{\partial \ell}\ \ell \qquad \text{(A-1)}$$

where ℓ is the length along a section perpendicular to the coastline and terminating at the 2000 m depth contour, it is possible to estimate e_N on this basis at all points west of the 2000 m contour. The correlation coefficients obtained for such linear regression analysis are always above .99.

Figure A-1 shows a plot of

$$e_{\zeta_s} = D - e_N \qquad \text{(A-2)}$$

where D is the quantity plotted in Figure 14. e_{ζ_s} is an estimate of the quasi-stationary component of the SST for the epoch July 1975 to August 1976. One data point has been eliminated, as shown on Figure A-1. The contours are in reasonable agreement with the expected flow of the Gulf Stream, given the approximate nature of the technique used.

The object of this note is to show that the quasi-stationary topography is recoverable from GEOS-3 altimetry if properly referred to a geoidal model of adequate precision. It also shows that present-day gravimetric geoids for the region are inadequate for this purpose. Procedures of the type described above (e.g., Leitao et al. 1977) are based on assumptions outlined in the preceding development and do not constitute a reliable basis for the determination of quasi-stationary SST.

8.2 Correlations from Overlapping Pass Analysis with Eddies

See Section 4. The residuals of fit (v_s in equation 12) to the mean surface for each overlapping pass, contains information on variations in sea surface height with wavelengths between 2 ℓ and the Nyquist limit. Typical eddy features are expected to have half wavelengths between 50 and 100 km, amplitudes up to 10^2 cm and a decay period of 10^2 days The data in Table 2 indicates that sea surface topography variations with amplitudes greater than 30 cm can be recovered with confidence.

A high pass filter corresponding to wavelengths greater than 100 km was applied to profiles of v_s listed in 32 sets in Table 2. The altimeter profiles which crossed an eddy reported in (NOAA 1975; NOAA 1976) for the periods September to December 1975 and April 1976, were examined through the window obtained for equivalent features in the profiles. The resulting altimeter defined sea surface topography variations are shown in Figures 18 to 22. The symbol H is used to designate anti-cyclonic eddies which should be associated with a SST high, while the symbol L is used to designate cyclonic eddies which are expected to be associated with a low in the SST.

Thirty-seven comparisons were made over a period of 7 months. Fifty-eight percent of these comparisons between altimeter and infrared data correlated favourably. A further 40 percent of the comparisons showed a partial overlap between the feature as sensed from the two data types. Only 2 percent of the comparisons did not correlate at all. These results are in substantial agreement with the results obtained from regional solutions (Table 6) which are subject to slightly higher levels of uncertainty.

Table 1

Regional Monthly Solutions for the Shape of the Sargasso Sea from GEOS-3 Altimetry

$25°N \leqslant \phi \leqslant 37°N$ $282°E \leqslant \lambda \leqslant 294°E$

Basic Junction Point Size — 0.2° x 0.2°

	Period		No of Obsns.	No. of Passes	No. of Jn. Pts	(± cm)*
1	April	1975	587	4	8	12
2	May	1975	821	6	13	12
3	June	1975	620	5	7	38
4	July	1975	2058	15	63	40
5	August	1975	2836	23	97	50
6	September	1975	3446	28	156	35
7	October	1975	4225	35	243	29
8	November	1975	3578	28	175	26
9	December	1975	1399	10	27	15
10	January	1976	—	—	—	—
11	February	1976	705	5	7	5
12	March	1976	560	4	4	8
13	April	1976	2205	19	63	17
14	May	1976	2092	16	70	19
15	June	1976	3195	25	140	26
16	July	1976	3089	22	122	20
17	August	1976	3093	24	131	22

*Equation 3

Table 2

Statistics For Overlapping Pass Sets

Set No	Rev No	Date YY	Date DDD	DIRN	Length (km)	Start of Overlap ϕ	Start of Overlap λ	No of Pts	Bias (m)	Tilt (arc sec)	$\delta\lambda\phi=0^\circ$ (km)	RMS Residual (± cm) $\partial N/\partial\lambda=0$	RMS Residual (± cm) $\partial N/\partial\lambda\neq0$	% Data Rejected
1	183	75	112	NS	2205	43 19	293.94	248	-0 53	-0 300	0	32.8	32 8	
	1235		187	NS	2176	43 19	293.94	245	4 12	-0 412	-12	33 7	35 8	
	2813		296	NS	2168	43 19	293.94	244	0 52	0 230	-21	47 1	42 4	
	4917	76	82	NS	2189	43 14	293.90	246	-4 09	0 041	-5	28 7	30 4	
	5443		119	NS	2077	43 14	293.90	234	-4.36	0 090	2	22 2	20.2	
	5969		156	NS	2182	43 03	293 80	245	4 39	0 315	11	32 2	32 8	
2	183	75	112	NS	1036	24.08	278 58	83	-3 57	-0 270	0	21 2	—†	2%
	1235		187	NS	1018	24 08	278.58	81	-0.82	-0 231	-12	18 4	—	2%
	2287		261	NS	1036	24 08	278 58	83	-2 73	0 484	-20	26.9	—	2%
	2813		298	NS	1027	24 08	278.58	82	1 62	0 567	-21	27 2	—	2%
	4917	76	82	NS	1036	24 08	278 58	83	-3 37	0 065	-5	20 4	—	2%
	5969		156	NS	1016	23.96	278.50	81	7 71	0 105	11	34.3	—	
3	246	75	117	SN	1994	20.20	290 66	214	0.56	0 258	0	44 5	44 5	
	1824		228	SN	1617	22 53	289 21	181	-2 06	0 127	-17	24 4	26 8	
	2876		303	SN	1628	22.37	289 31	180	-0.50	0 110	-20	25 4	33.4	
	3402		340	SN	238	31 24	283 30	30	-1.00	-0 297	-18	22 6	23 4	
	6032	76	161	SN	1932	20.20	290 66	206	-0 04	0 105	14	57 0	51 2	
	7084		235	SN							36			
4	374	75	126	SN	1456	22 02	288 15	152	-3 61	0 108	0	29 7	29 7	
	2478		275	SN	1404	22 02	288 15	149	0 07	0 090	-18	37 6	23 0	3%
	3004		312	SN	1404	22 02	288 15	149	0 99	0 026	-18	36 6	17 0	3%
	6160	76	170	SN	1456	22 02	288 15	152	-0 64	-0 036	18	36 6	16 4	3%
	6686		207	SN	1427	22 19	288.04	149	3 02	-0 194	29	60.9	28 1	
	7212		244	SN							41			
5	524	75	137	NS	2990	44.87	300.56	358	2 48	-0 086	0	25 3	25 3	
	1576		211	NS	2967	44 73	300 40	355	-0 77	-0 093	-11	29 7	29 7	4%
	2678		285	NS	121	26.84	285 16	15	0 16	0 206	-16	7 6	8 3	
	3154		322	NS	2983	44.83	300 51	357	0.92	-0 105	-16	42 3	39 8	
	5258	76	106	NS	2990	44.87	300 56	358	-3.20	-0 008	4	22 0	25 8	
	6310		181	NS	2967	44 73	300 40	355	-1 30	0 181	23	31 8	31.5	
	6836		218	NS	2975	44 78	300 45	356	1 88	0 109	34	41 1	40 2	
6	530	75	137	SN	1490	27 73	293.97	183	-1.54	-0 088	0	23 2	23 2	
	2108		248	SN	1450	27 89	293 86	178	3 32	-0 101	-14	21 3	19 1	
	3160		323	SN	1483	27 73	293.97	182	0.96	0 010	-16	25 0	23.9	
	5264	76	107	SN	1465	27.89	293 86	180	2 49	-0 091	4	22 8	23 8	
	6316		181	SN	1465	27 89	293 86	180	-2 47	0 000	23	22 4	21 3	
	6842		218	SN	1441	28 05	293 75	177	-1 74	0 132	34	27.9	19 7	
7	587	75	141	SN	1553	25 62	291.97	187	-4 51	-0 080	0	23 0	23 0	
	2165		253	SN	1369	26 11	291.64	166	0 36	0 373	-14	17 4	17 1	
	2691		290	SN	1522	25 62	291.67	183	0 36	-0 102	-15	21 2	19 1	
	5321	76	111	SN	1553	25 62	291 67	187	4 67	-0 161	5	17 0	16 2	
	5847		148	SN	1536	25 73	291.89	185	-0 77	-0 008	14	17 5	19.9	
	6373		185	SN	1552	25 62	291.97	187	0 25	-0 039	25	29.5	23 6	
8	595	75	142	NS	5300	46 67	304 74	534	-2 00	0 065	0	29 8	29 8	1%
	1121		179	NS	5300	46 67	304 74	534	-0 18	-0 010	-6	29 5	34 0	1%
	1647		216	NS	5300	46 67	304 74	534	-7 47	0 014	-11	50 7	49 7	1%
	2173		253	NS	5001	44 89	302 65	527	5 71	-0 348	-14	38 5	37 5	1%
	2699		290	NS	4993	44.84	302 60	526	2 57	0 136	-15	39 2	34 6	
	3751		365	NS	4993	44.84	302 60	526	-3 48	-0 022	-12	33 4	32 2	1%
	5329	76	111	NS	5300	44 67	304 74	534	-2 10	0 039	6	37 0	38 5	1%
	5855		148	NS	5001	44 89	302 65	527	5 08	0 068	15	38 4	30 8	
	6381		186	NS	4972	44.89	302 65	524	2 37	0 010	25	55 3	44 1	

†Data bank errors

Table 2 (continued)

Set No	Rev No	Date YY	Date DDD	DIRN	Length (km)	Start of Overlap ϕ	Start of Overlap λ	No of Pts	Bias (m)	Tilt (arc sec)	$\delta\lambda\ \phi=0^\circ$ (km)	RMS Residual (± cm) $\partial N/\partial\lambda=0$	RMS Residual (± cm) $\partial N/\partial\lambda\neq0$	% Data Rejected
9	837	75	159	NS	2161	44 88	294 40	261	-3 21	0 136	0	53 4	53 4	
	1363		196	NS	2111	44 79	294.29	265	-2 52	0 276	-5	57 9	57 2	
	2415		270	NS	2040	44.88	294 40	249	-2 82	-0 065	-12	41 4	34 2	
	2941		307	NS	2118	44.88	294 40	256	6 58	-0 779	-12	73 5	74 2	
	6097	76	165	NS	1984	43 76	293 16	244	4 50	-0 093	22	61 1	33 5	
	6623		203	NS	1969	43 66	293 06	242	-0.24	-0 064	33	70 7	24.3	
	7149		240	NS							45			
10	837	75	159	NS	1188	24.99	277 74	111	-2 13	0 099	0	24 6	24 6	5%
	1363		196	NS	1188	24.99	277 74	111	-0 71	0 213	-5	19 5	23 5	5%
	2941		307	NS	1188	24 99	277 74	111	-1 87	-0 451	-12	18 8	27 0	5%
	6097		165	NS	1133	24 78	277 70	105	5.55	-0 151	22	23 7	36 3	2%
	6623		203	NS	1134	24 67	277 53	105	-0.96	0 017	33	26 9	33 5	
	7149		240	NS							45			
11	843	75	159	SN	1614	23 67	290 47	185	-10 85	-0 627	0	28 1	28 1	
	1369		196	SN	1545	24 10	290 19	177	2 10	0 123	-6	21 7	20 2	
	1895		233	SN	247	23 67	290 47	27	4 23	-0 302	-10	10 9	10 8	
	2421		271	SN	1554	24.05	290 22	178	0 46	0 131	-12	31 9	30 5	
	2947		308	SN	1614	23 67	290 47	185	2 84	0 173	-13	29 7	25 0	
	4525	76	54	SN	1614	23 67	290 47	185	3 78	-0 010	-2	27 1	26 1	
	6103		166	SN	1563	23.99	290.26	179	-1 87	0 217	23	38 0	31 4	
	6629		203	SN	1571	23 94	290 29	180	2 08	0 052	34	43 3	31 2	
12	851	75	160	NS	2091	28 58	285 66	193	30 82	-1 103	0	44 8	—— †	1%
	1377		197	NS	1947	28 58	285 66	178	-4 40	0 433	-6	41.2	——	
	1903		234	NS	2082	28 58	285 66	192	-18 53	-0 905	-10	44 6	——	3%
	2429		271	NS	2072	28.58	285 66	191	-3.01	0 499	-12	37 9	——	3%
	2955		308	NS	2082	28 58	285 66	192	-4 05	-0 139	-12	38 9	——	
	3481		346	NS	2082	28 58	285 66	192	-4 18	0 330	-11	40 8	——	2%
	6111	76	166	NS	2091	28 58	285 66	193	4 30	0 439	23	76 7	——	1%
	6637		204	NS	2091	28 58	285 66	193	-0 55	0 255	34	114 4	——	1%
	7163		241	NS							46			
13	1164	75	182	NS	711	36 59	285 60	85	-43 11	-0 461	0	59 3	59 3	15%
	2216		256	NS	590	36 02	285 12	72	8 45	-0 210	-8	20 9	22 1	4%
	3268		330	NS	566	35.87	285 00	69	11 11	-0 002	-8	20 1	20 7	
	4846	76	77	NS	711	36 59	285 60	85	5 36	-0 733	6	46 9	43 2	15%
	5372		114	NS	711	36 59	285 60	85	9 76	-0 677	13	56 7	46 0	15%
	5898		151	NS	711	36 59	285 60	85	15 85	-0 751	23	65 8	47 6	15%
	6950		226	NS							45			
14	1164	75	182	NS	1164	25 44	277 31	129	-43 61	0 776	0	43 5	43 5	5%
	2216		256	NS	1126	25 44	277 31	125	8 18	-0 012	-8	36 6	40 0	2%
	3268		330	NS	1126	25 44	277 31	125	11 09	-0 025	-8	36 9	39 8	2%
	4846	76	77	NS	662	25.39	277 27	75	4 40	-0 508	6	45 2	43 7	1%
	5372		114	NS	1119	25 17	277 14	124	7 05	0 503	13	80 5	80 9	2%
	5898		151	NS	1146	25 34	277 24	127	13 03	0 383	23	54 4	52 3	5%
	6950		226	NS							45			
15	1170	75	182	SN	705	29 12	286 07	81	4 03	-1.530	0	26 4	26 4	
	2222		257	SN	553	29 12	286 07	62	-0 73	0 495	-8	24 4	17 3	
	2748		294	SN	697	29 12	286.07	80	-0 14	0 272	-9	23 5	17 3	
	4852	76	77	SN	705	29 12	286 07	81	0 45	0 431	6	18 4	15 5	
	5904		152	SN	705	29 12	286 07	81	-3 94	0 454	23	31 5	20 7	
	6956		226	SN							45			

Table 2 (continued)

Set No	Rev No	Date YY	Date DDD	DIRN	Length (km)	Start of Overlap ϕ	Start of Overlap λ	No of Pts	Bias (m)	Tilt (arc sec)	$\delta\lambda\,\phi=0^{\circ}$ (km)	RMS Residual (± cm) $\partial N/\partial\lambda=0$	RMS Residual (± cm) $\partial N/\partial\lambda\neq 0$	% Data Rejected
16	1178	75	183	NS	4640	44.87	299 13	469	-2.25	-0 001	0	32 2	— †	1%
	2230		257	NS	4596	44 72	298 96	464	-1.56	-0 001	-8	39 4	—	
	2756		294	NS	4630	44 87	299 13	468	3 26	-0 112	-9	44 3	—	1%
	4860	76	78	NS	4615	44 72	298.96	466	-4 72	-0.002	6	27 8	—	
	5386		115	NS	4624	44 77	299 02	467	-3 52	-0 041	14	27 0	—	
	5912		152	NS	4640	44.87	299 12	469	6 64	0 115	23	36 2	—	1%
	6438		190	NS	3517	44.82	299 07	371	3 17	-0 045	33	49 7	—	1%
	6438		190	NS	663	20 51	279 64	72	1 56	1 302	33	38 3	—	
17	1440	75	301	SN	1558	25 14	291 50	161	6 56	-0 544	0	22 1	22 1	1%
	1966		238	SN	1558	25 14	291 50	161	-1 17	0 100	-4	21 5	21 6	1%
	2492		276	SN	1558	25 14	291.50	161	0 89	0 026	-6	18 9	19 4	2%
	3018		313	SN	1535	25 19	291 47	158	-2 82	0 139	-6	23 8	24 3	
	4596	76	59	SN	1558	25 14	291.50	161	-0 15	0 058	5	19 1	19 3	2%
	6174		171	SN	1523	25 36	291 35	157	-3.32	0 169	31	32 4	17 7	
	6700		208	SN							42			
	7226		245	SN							54			
18	1562	75	210	NS	2081	43 61	293 60	237	0 46	0 020	0	30 4	30 4	
	2088		247	NS	2073	43 56	293 55	236	1 25	-0 282	-3	37 8	36 5	
	3140		321	NS	2064	43 61	293 60	235	-2 55	-0 046	-5	26 4	27 8	
	3666		359	NS	2081	43 61	293 60	237	-0 49	-0 143	-2	34 6	37 1	
	5770	76	142	NS	2042	43.37	293 34	232	1 58	0 409	24	31 9	24 7	
	6822		217	NS							45			
19	1562	75	210	NS	258	24 63	278 10	26	0 94	0 311	0	72 0	72 0	
	2088		247	NS	258	24 63	278 10	26	-2 76	-0 167	-3	70 1	69 2	
	3140		321	NS	258	24 63	278 10	26	-1 41	-0 112	-5	70 8	74 3	
	3666		359	NS	258	24 63	278 10	26	-0 35	-0 002	-2	65 1	73 2	
	5770	76	142	NS	142	24 20	277.82	17	5 13	1 304	24	11 5	— †	
	6822		217	NS							45			
20	1568	75	210	SN	1607	24 13	290 77	183	0 23	0 026	0	26 1	26 1	
	2094		247	SN	1607	24 13	290 77	183	1 95	-0 296	-3	26 3	26 2	
	2620		285	SN	1565	24.35	290 63	178	-0.53	-0 102	-5	20 2	18 1	
	3146		322	SN	1599	24 13	290 77	182	0 54	-0 078	-5	24 7	23 2	
	5776	76	143	SN	1590	24.24	290 70	181	1 10	0 111	24	25 3	23 1	
	6302		180	SN	1590	24 24	290 70	181	-3 41	0 369	34	32 6	29 9	
	6828		217	SN							46			
21	1625	75	214	SN	1510	22 36	288 48	165	-0 78	0 058	0	21 0	21 0	
	2151		252	SN	1502	22 36	288 48	164	2 16	-0 308	-3	24 4	22 6	
	2677		289	SN	1478	22 36	288 48	163	-1 58	0 013	-5	20 1	18 3	
	3203		326	SN	1478	22 36	288 48	163	-1 94	0 058	-4	26 7	23 0	
	3729		363	SN	1502	22 36	288 48	164	-1 33	0 108	-2	32 3	30 9	
	5307	76	110	SN	1510	22 36	288 48	165	0 11	0 066	17	36 2	22 1	
	5833		147	SN	1510	22 36	288 48	165	3 43	-0 041	26	46 8	25 5	
	6885		221	SN							47			
22	1682	75	218	SN	1973	15 14	289 41	180	-0 25	0 020	0	35 2	35 2	1%
	2208		256	SN	1965	15 14	289 41	179	-1 76	-0 003	-3	38 8	39 9	2%
	3260		330	SN	1963	15 20	289.37	179	2 50	-0 350	-3	39 7	47 2	1%
	5364	76	114	SN	1121	20 21	286 39	112	-0 21	-0 103	18	40 1	29 1	1%
	6416		188	SN	1103	20 32	286 32	110	0 51	0 519	38	106 3	49 8	
	6942		225	SN							49			

Table 2 (continued)

Set No	Rev No	Date YY	Date DDD	DIRN	Length (km)	Start of Overlap ϕ	Start of Overlap λ	No of Pts	Bias (m)	Tilt (arc sec)	$\delta\lambda\ \phi=0^\circ$ (km)	RMS Residual (± cm) $\partial N/\partial\lambda=0$	RMS Residual (± cm) $\partial N/\partial\lambda\neq0$	% Data Rejected
23	1710	75	220	SN	1508	26 82	293 09	152	0 85	-0 051	0	26 7	26 7	
	2236		258	SN	1508	26.82	293.09	152	0 78	0 219	-3	28 1	27 0	
	2762		295	SN	262	31 24	289.96	28	0 08	-0 025	-4	12 8	12 3	
	2762		295	SN	40	36 37	285 91	6	-0 49	0 729	-4	15.8	18 1	
	5392	76	116	SN	1508	26.82	293 09	152	1 48	-0 205	19	20 9	28 5	
	5918		153	SN	332	33 48	288 26	28	-1 62	-0 438	28	15 3	11 8	
	6444		190	SN	1490	26.94	293 01	150	-1.82	-0 112	38	31.8	28 1	
	6970		227	SN							50			
24	1789	75	226	NS	992	25 73	290 45	105	3 06	-0 127	0	33 1	33 1	
	2315		263	NS	992	25 73	290 45	105	-1 31	-0 165	-3	38 5	44 3	
	2841		300	NS	992	25 73	290 45	105	-0 28	-0 009	-3	32.9	33 7	3%
	4945	76	84	NS	973	25 73	290 45	103	-0 81	0 062	13	41 3	24 8	3%
	5471		121	NS	946	25 73	290 45	100	-0 60	-0 048	21	43 0	24 5	6%
	7049		233	NS							53			
25	1810	75	227	SN	1105	19 36	285 53	95	-0 54	0 214	0	38 4	38 4	
	2336		265	SN	1105	19.36	285 53	95	3 02	-0 347	-2	48 8	47 4	
	2862		302	SN	1105	19 36	285 53	95	-1 37	0 307	-3	34 6	32 5	
	3388		339	SN	493	23 04	283 24	43	-0 84	-0 018	-2	25 4	26 5	
	5492	76	123	SN	1086	19 47	285 47	93	-2 22	0 247	21	52 6	31 4	
	6018		160	SN	348	19 47	285 47	23	-0 83	0 129	31	99 7	39 8	
	7070		234	SN							53			
26	1846	75	230	NS	1825	25 87	287 12	157	1 65	-0 310	0	40 7	40 7	2%
	2898		304	NS	1825	25 87	287 12	157	-5 51	-0 708	-3	50 1	47.9	2%
	5528	76	125	NS	1797	25 87	287 12	154	-2 20	0 204	22	35 5	24 6	2%
	6054		162	NS	1797	25 87	287 12	154	4 64	0 234	32	48 8	35 7	
	6580		200	NS							42			
	7106		237	NS							54			
27	1974	75	239	NS	4481	41 96	298 71	468	2 95	-0 369	0	31 4	31 4	
	2500		276	NS	4471	41 96	298 71	467	4 08	0 222	-2	39 8	38 8	
	3026		313	NS	4462	41.96	298 71	466	-0.27	-0 109	-2	31 0	30 6	
	3552		351	NS	4471	41.96	298 71	467	-0 78	-0 108	0	34 3	34.9	
	4604	76	60	NS	3036	41.96	298 71	343	-4 71	0 001	9	24 0	27 2	
	6182		171	NS	4481	41.96	298 71	468	1 57	-0 172	35	63 7	49 7	
	6708		209	NS							46			
	6708		209	NS							46			
	7234		246	NS							58			
28	2037	75	243	SN	1526	26 35	292 70	173	2 62	-0 430	0	26 2	26 2	
	2563		281	SN	1526	26 35	292 70	173	0 03	-0 035	-2	20 1	20 3	
	3089		318	SN	1526	26.35	292 70	173	0 60	-0 088	-2	20.2	19 8	
	5193	76	102	SN	1480	26 41	292 67	167	2 28	0 014	18	18 7	26 3	
	5719		139	SN	1518	26 41	292 67	172	-1 26	-0 018	26	19 7	23 0	
	6245		176	SN	1501	26.52	292 60	170	-2 31	0 050	36	27 0	20 1	
29	2159	75	252	NS	4315	44.35	296 43	438	-5 06	-1 022	0	102 8	—†	
	3211		326	NS	4315	44 35	296 43	438	3 28	0 132	-1	66 7	—	
	3737		364	NS	4315	44 35	296 43	438	2 72	0 047	2	49 0	—	
	5315	76	110	NS	4315	44 35	296 43	438	-1 67	0 236	20	68 3	—	
	5841		147	NS	235	44 21	296 27	33	3 80	0 312	29	18 9	—	
	5841		147	NS	3038	36 43	288 81	284	6 38	0 260	29	65 8	—	
	6893		222	NS							51			

Table 2 (continued)

Set No	Rev No	Date YY	Date DDD	DIRN	Length (km)	Start of Overlap ϕ	Start of Overlap λ	No of Pts	Bias (m)	Tilt (arc sec)	$\delta\lambda\ \phi=0^{\circ}$ (Km)	RMS Residual (± cm) $\partial N/\partial\lambda=0$	RMS Residual (± cm) $\partial N/\partial\lambda\neq 0$	% Data Rejected
30	2464	75	274	SN	1130	18 57	284 61	89	-1 74	-0 157	0	38 2	38 2	4%
	3516		348	SN	213	18 67	284 61	22	-0 04	-0 549	2	19 4	21 5	
	3516		348	SN	532	22 09	282 45	59	-1 10	0 682	2	15 4	16 4	
	4568	76	57	SN	1130	18.57	284 61	89	0 52	-0 112	10	27 6	37 4	
	6146		169	SN	1066	18 95	284 38	84	1 49	-0 155	36	57.9	32 2	8%
	7198		243	SN							59			
31	2486	75	275	NS	2392	43.51	294.81	257	2 72	-0 045	0	24 5	24 5	
	3012		312	NS	2346	43 51	294 81	252	3 10	0 011	0	38 3	40 0	
	4590	76	59	NS	2392	43 51	294.81	257	-2 07	-0 030	11	22 9	26 1	
	5116		96	NS	2384	43 46	294 76	256	-2 72	0 050	18	21 6	25 9	
	5642		133	NS	2392	43 51	294 81	257	-1 19	0 057	27	34 4	29 0	
	6694		208	NS							48			
	7220		245	NS							60			
32	2506	75	277	SN	1431	28 72	294 48	167	1 79	0 330	0	26 2	26 2	
	3558		351	SN	1423	28 72	294 48	166	0 00	-0 089	2	27 8	28 2	
	4610	76	60	SN	1431	28 72	294 48	167	1 64	-0 130	11	20 4	21 5	
	5136		98	SN	1423	28 78	294 44	166	0 64	-0 138	19	19.8	22 6	
	5662		135	SN	1406	28 88	294.36	164	-0 71	-0 133	27	16 4	21 9	
	6188		172	SN	1366	29 15	294 18	159	-1 68	-0 054	37	21 8	25 4	

Table 3

Residual Noise (σ in Equation 3) as a Function of Junction Point Size

Junction Point (Crossover) Size (Degrees)	Root Mean Square Residual (± cm)
0.2° x 0 2°	20
0 5° x 0 5°	52
1° x 1°	78

Table 4

The Effect of Allowing for the Ocean Tide on the Root Mean Square Residual (σ) for a Monthly Solution in the Sargasso Sea

Tidal Model — Hendershott Month — October 1975

For more details, see Table 1, Row 7 and Figure 15

Solution Description	σ (± cm)	Mean Sea Surface Height at 243 Junction Points (m)
Tide Not Modelled	29	-49.36
Tide Modelled	29	-49.33

Table 5

Three Parameter Transformations of Regional Sea Surface Models to the GEM 9 Datum

Equation 4			GEM 9 to (30,30)	
Solution Description		Meridional Tilt (+ N) cm per 10 km	Prime Vertical Tilt (+ E) cm per 10 km	Radial Correction (m)
July	1975	-4	+1.5	+0 7
August	1975	-6	+2 5	+1.7
September	1975	-5 5	+3	-2 8
October	1975	-5	+4	-3.6
November	1975	-5 5	+3.5	+1.4
April	1976	-5	+5	+1 8
May	1976	-4.5	+4.5	+1 6
June	1976	-5 5	+4.5	+1 5
July	1976	-5.5	+5	+1.5
August	1976	-5	+4.5	+1.5

Table 6

Correlations Between Remote Sensed Cyclonic Eddies/Monthly Surface Temperature Means and Dynamic Sea Surface Heights of Regional Models of the Sargasso Sea from GEOS-3 Altimetry

Month	Year	No of Passes	No of Junction Points	RMS Residual After Adjustment (±m)	% of Data Rejected	Correlations With Cyclonic Eddies as (%) function of distance d(km)*					Correlations With Monthly Surface Temperature Mean Maxima and Minima Defined in Four Cardinal Directions				
						0≤d≤50	(%) 50≤d≤100	d>100	Insuff Data	Sample Size	Positive**	(%) Favorable**	Negative**	No Data	Sample Size
July	1975	15	63	0 40	0	100	–	–	–	2	–	–	–	–	–
August	1975	23	97	0 50	18	67	–	–	33	3	67	–	17	16	6
September	1975	28	156	0 35	8	75	25	–	–	4	40	40	–	20	5
October	1975	35	243	0 29	2	75	25	–	–	4	67	16	17	–	6
November	1975	28	175	0 26	1	50	25	–	25	4	43	–	–	57	7
April	1976	19	63	0 17	6	50	25	–	25	4	40	–	20	40	5
May	1976	14	59	0 21	1	50	50	–	–	2	40	–	20	40	5
June	1976	25	140	0 26	2	–	100	–	–	1	33	33	–	34	3
July	1976	22	122	0 20	–	67	33	–	–	3	50	–	50	–	4
August	1976	24	131	0 22	–	75	–	–	25	4	50	–	25	25	4
				Total		64	24	–	12	33	50	9	16	25	44

*Correlations established from relative sea surface height variations along profiles over eddy locations reported in (NOAA 1975, NOAA 1976)

**Positive correlation defined by occurrence of highs or lows of same sign in both altimeter sea surface models and in surface temperature means for $1^{\circ} \times 1^{\circ}$ squares (ibid)
Positive = exact correlation in four cardinal directions or ground track directions if available
Favorable = exact correlation along three out of four cardinal or ground track directions
Negative = exact correlation along less than three out of four cardinal or ground track directions

Table 7

The Variation of Specific Volume of Sea Water With Temperature

Temperature °C	$(\partial\alpha/\partial T) \times 10^{-4}$ · $cm^3\ g^{-1}\ (°K)^{-1}$
0	3.19
5	3.14
10	3.08
15	3.03
20	2.98
25	2.93
30	2.88
35	2.83
40	2.78

Table 8

Spectral Analysis of Overlapping Pass Set 8 (Table 2)

Rev No / Range of Wavelength		595			1121			1647			2173			2699			3751			5329			5865			6381			Mean for Set 8				
	Nt	Ot	E1	St	O	E	S	O	E	S	O	E	S	O	E	S	O	E	S	O	E	S	O	E	S	O	E	S	O	σ	E	σ	Ratio
25	59	29	20,3		39	20 3		16	20.3		57	24 0		75	24 0		73	24 0		30	20 3		58	24 0		40	24 1		4 63	2 05	22 37	1 97	0 21
50	103	9.8	39 8		73	39 8		46	39 8		73	38 0		100	38 0		103	38 0		87	39 8		107	38 0		102	37 9		8 77	2 01	38 86	0 95	0 23
75	35	20	13 5		42	13 5		34	13 5		57	12 9		42	12 6		74	12 6		41	13 5		54	12 9		38	12 6		4 57	1 38	13 09	0 43	0 35
100	17	24	6 4		28	6 4		22	6 4		35	6 1		32	6 5		32	6 5		41	6 4		46	6 1		63	6 5		3 59	1 27	6 36	0 16	0 56
125	10	6 3	4 1		44	4 1		30	4 1		29	3 8		50	3 8		36	3 8		56	4 1		33	3 8		47	3 8		4 31	1 20	3 96	0 17	1 09
150	7	6 9	2 6		34	2 6		55	2 6		54	2 7		74	2 3	**	57	2 3	*	31	2 6		72	2 7	**	84	2 3	*	5 89	1 79	2 52	0 17	2 33
175	5	3 3	1 9		39	1 9		33	1 9		49	1 9		105	1 9	***	59	1 9	**	33	1 9		46	1 9	**	104	1 9	*	5 57	2 9	1 90	0 02	2 93
200	4	7 1	1 5	***	50	1 5		44	1 5	*	23	1 1		32	1 6	*	34	1 5	*	70	1 5	**	43	1 1		34	1 5	**	4 46	1 67	1 42	0 17	3 14
225	3	3 3	1 1		39	1 1	**	23	1 1		18	1 1		06	0 8		04	0 8		19	1 1		10	1 1		05	0 8		1 74	1 26	1 01	0 19	1 73
250	2	4 3	0 8	*	07	0 8		24	0 8	***	03	0 8		66	1 1	* *	19	1 1		30	0 8	*	14	0 8		17	1 1		1 96	1 96	0 89	0 20	2 20
275	2	2 5	0 8	**	08	0 8		15	0 8		21	0 8		07	0 4		03	0 4		25	0 8	**	45	0 8	*	01	0 4		1 67	1 40	0 63	0 19	2 65
300	2	4 8	0 8		13	0 8		16	0 8		28	0 8	**	08	0 8		17	0 8		48	0 8	**	25	0 8	***	27	0 8	*	2 56	1 43	0 76	0 01	3 36
325	1	3 5	0 4	***	12	0 4	*	17	0 4		03	0 4		07	0 4		02	0 4		11	0 4	*	01	0 4		21	0 4	* *	1 21	1 10	0 38	0	3 19
350	1	0 6	0 4		06	0 4		12	0 4		09			00	0 4		00	0 4		08	0 4	*	04	0 4		09	0 4		0 60	0 41	0 38	0	1 58
375	1	0 8	0 4	*	10	0 4		01	0 4		11	0 4	*	04	0 4		12	0 4	*	24	0 4	*	09	0 4	*	06	0 4		0 84	0 65	0 38	0	2 48
400	1	2 0	0 4		18	0 4	**	09	0 4	*	26	0 4	**	11	0 4	**	09	0 4		21	0 4	*	20	0 4	***	19	0 4		1 73	0 63	0 38	0	4 56
425	1	1 5	0 4	*	28	0 4	*	26	0 4	*	24	0 4	***	10	0 4		19	0 4	* *	01	0 4		15	0 4	*	14	0 4	**	1 69	0 85	0 38	0	4 44
450	1	0 2	0 4		31	0 4		06	0 4											06	0 4								1 12	1 33	0 38	0	2 96
475	1										02	0 4		35	0 4	*	44	0 4					27	0 4	*	55	0 4		3 26	2 00	0 38	0	8 58
500	1	1,2	0 4	***	23	0 4		16	0 4					73	0 4		18	0 4	**	18	0 4					24	0 4	**	2 63	2 10	0 38	0	6 92
525	1										43	0 4											17	0 4	***				30	1 84	0 38	0	7 9
550	1	4,3	0 4		29	0 4		24	0 4	*										45	0 4	***							3 53	1 03	0 38	0	9 28
575	1										20	0 4	*	02	0 4		43	0 4					29	0 4		24	0 4	**	2 36	1 49	0 38	0	6 21
600	1	2 7	0 4	**	64	0 4		50	0 4											05	0 4								3 65	2 60	0 38	0	9 60
625	1													33	0 4	*	11	0 4								11	0 4	*	1 83	1 27	0 38	0	4 82
650	1										11	0 4											42	0 4	*				2 65	2 19	0 38	0	6 97
675	1	0 5	0 4		07	0 4		17	0 4											13	0 4	***							1 05	0 55	0 38	0	2 76
725	1										16	0 4		09	0 4	*	05	0 4					21	0 4	**	04	0 4		1 10	0 73	0 38	0	2 90
775	1	0 2	0 4		21	0 4		04	0 4											33	0 4	*							1 50	1 47	0 38	0	3 95
850	1										36	0 4	*	43	0 4		71	0 4					05	0 4		24	0 4		3 58	2 44	0 38	0	9 42
900	1	5 3	0 4	*	20	0 4	*	10	0 4											50	0 4	*							3 32	2 15	0 38	0	8 75
1000	1													5,4	0 4		39	0 4	*							47	0 4	**	4 67	0 75	0 38	0	12,28
1025	1										44	0 4											07	0 4					2 55	2 62	0 38	0	6 71
1075	1	3 0	0 4	*	22	0 4		40	0 4											16	0 4	* *							2 70	1 04	0 38	0	7 1
1250	1													78	0 4		50	0 4	*							87	0 4	*	5 5	2 10	0 38	0	14 47
1275	1										44	0 4											88	0 4	**				6 6	3 11	0 38	0	17 37
1350	1	1 6	0 4		61	0 4		15	0 4											02	0 4								2 35	2 58	0 38	0	6 18
1675	1										40	0 4		30	0 4	***	56	0 4	*				40	0 4	*	30	0 4		3 92	1 06	0 38	0	10 32
1775	1	2 2	0 4	*	64	0 4		07	0 4											03	0 4								2 40	2 79	0 38	0	6 32
2500	1													03	0 4		103	0 4								47	0 4		5 1	5 01	0 38	0	13 42
2525	1										65	0 4	**										52	0 4	*				5 85	0 92	0 38	0	15 40
2675	1	2 1	0 4		27	0 4		37	0 4											43	0 4								3 2	0 99	0 38	0	8 42
4975	1																									67	0 4		6 7	-	0 38	0	17 63
5000	1													11	0 4		09	0 4											1 0	0 14	0 38	0	2 63
5025	1										161	0 4	*										69	0 4					11 5	6 5	0 38	0	30 26
5325		11 7	0 4		143	0 4		350	0 4											186	0 4								19 9	10 46	0 38	0	52 36

tN number of frequencies per bin
tO = observed strength of signal (Eqn 14)
E = expected contribution per bin assuming flat white noise spectrum (Eqn 13)
S = significance of the signal >1σ >2σ >3σ

Table 9

Spectral Analysis of 32 Sets of Overlapping Passes in Western North Atlantic
(For Description of Headings See Footnote of Table 8).

Set No	1				2				3				4				5				6				7				8				9			
Range of W L (km)	N	E	O	S	N	E	O	S	N	E	O	S	N	E	O	S	N	E	O	S	N	E	O	S	N	E	O	S	N	E	O	S	N	E	O	S
0	78	64	6	21	4				21	50	6	24	1				50	65	2	13	8				80	63	2	17	9				102	67	4	20	8
50	22	18	0	13	2				10	24	7	20	8				16	17	4	11	6				24	18	7	12	8				27	17	3	10	1
100	7	59	7	1	*				4	99	14	4	*				6	71		57					8	63		64					9	71		52	
150	4	30	3	8	*				1	25	3	5	*				3	28		74	**				4	31		45	*				5	28		35	*
200	2	18	3	5	**				1	25	7	1	**				2	33	15	1	***				2	15		27	*				3	17		46	**
250	2	17	3	8	**				1	25	9	5	***				2	21		51	**				2	15		46	***				2	11		34	***
300	2	17	3	7	**				1	25	8	9	***				2	20		67	***				1	08		31	***				1	06		10	*
350	1	08	3	6	***												1	10		15	*				1	08		65	***				1	06		36	***
400	2	17	4	8	**												1	11		53	***												2	11		77	***
450																	1	10		100	***	2	16	27	5	***				1	06		65	***
500	3	25	25	8	***	1	25	9	0	***	1	11		17	*	1	08		38	***	1	06		48	***											
600	1	09	16	0	***						2	19		342	***																					
700	2	16	10	4	***											1	08		58	***	1	06		61	***	2	20	16	0	***	2	20	11	0	***
800											1	11		81	***																					
900											2	19		165	***																					
1000	3	25	35	0	***	2	49	4	9							2	16		86	***	2	11	24	8	***	3	30	25	0	***	1	10		50	***
1500											4	42	12	10	***																					
2000	4	33	77	4	***											2	16	45	5	***																
2500																					2	11	26	6	***											
3000																																				
3500																																				
4000																																				
4500																																				
5000																																				
>5000																																				

Table 9 (continued)

Set No	10				11				12				13				14				15				16				17				18			
Range of W L (km)	N	E	O	S	N	E	O	S	N	E	O	S	N	E	O	S	N	E	O	S	N	E	O	S	N	E	O	S	N	E	O	S	N	E	O	S
0	21	58	0	166	52	65	7	240	54	57	0	144	27	67	1	131	37	64	5	211	23	65	0	274	123	61	0	133	48	61	3	203	76	65	1	160
50	12	21	6	117	14	17	3	93	20	21	9	99	7	16	9	166	11	18	1	159	7	18	1	237 *	40	19	7	148	16	19	7	172	21	17	7	76
100	4	7	4	107 *	5	6	5	98 *	7	7	4	102 *	2	6	7	48	4	6	2	140 **	3	6	8	170 **	14	6	6	112 *	5	5	2	94 *	7	6	0	31
150	2	3	7	91 **	3	3	9	59 *	3	3	2	114 ***	1	2	6	41 *	2	3	4	94 **	2	5	3	142 **	7	3	2	84 **	3	3	8	89 **	3	2	6	45 *
200	1	1	9	70 ***	2	3	8	111 **	2	2	1	51 **	1	2	4	145 ***	2	3	7	139 ***	1	2	5	51 **	4	2	2	111 ***	1	1	3	34 **	2	1	7	33 *
250	1	1	9	52 **	1	1	1	54 ***	2	2	1	39 *	1	2	9	123 ***	1	1	6	59 ***	1	3	3	132 ***	3	1	2	45 ***	1	1	3	48 ***	2	1	7	58 ***
300					1	1	1	52 ***	2	2	2	202 ***					1	2	7	111 ***	1	2	6	64 **	2	1	2	49 ***	1	1	3	100 ***	1	0	9	35 ***
350	1	1	9	83 ***	1	1	1	31 **	1	1	1	59 ***	1	2	4	259 ***	2	3	2	182 ***	1	2	5	74 **	2	0	9	47 ***	1	1	3	62 ***				
400									1	1	1	51 ***													2	0	9	24 ***					1	0	9	51 ***
450									1	1	1	17 *													1	0	4	12 **								
500	2	3	7	319 ***	2	2	2	336 ***	1	1	1	27 **	2	5	8	206 ***	2	3	2	165 ***	1	3	3	135 ***	3	1	3	51 ***	1	1	3	61 ***	1	0	9	27 ***
600									2	2	2	126 ***					1	2	7	128 ***					1	0	8	43 ***					1	0	9	42 ***
700					2	2	2	76 ***					1	2	4	404 ***					2	5	1	220 ***	2	1	0	93 ***	2	2	5	118 ***				
800					1	1	1	61 ***																	1	0	5	180 ***								
900									1	1	1	195 ***													2	0	9	50 ***								
1000	2	3	7	320 ***					1	1	1	168 ***					3	4	8	489 ***					2	0	9	70 ***					2	1	7	371 ***
1500					3	3	3	395 ***	1	1	1	39 ***													2	1	0	54 ***	3	3	7	222 ***	3	2	5	675 ***
2000									2	2	1	98 ***													2	0	9	81 ***								
2500																																				
3000																																				
3500																									1	0	5	27 ***								
4000																																				
4500																									3	1	3	157 ***								
5000																																				
>5000																																				

Table 9 (continued)

Set No	19				20				21				22				23				24				25				26				27			
Range of W L (km)	N	E	O	S	N	E	O	S	N	E	O	S	N	E	O	S	N	E	O	S	N	E	O	S	N	E	O	S	N	E	O	S	N	E	O	S
0																																				
50	7	61	7	154	58	652	266		52	640	180		43	575	117		30	688	318		32	633	133		20	539	152		43	539	110		144	618	119	
100	3	241	84		16	178	155		15	180	120		16	216	144		11	210	131		10	191	161		9	242	198		18	234	145		45	194	60	
150	1	92	242	**	5	59	154	**	5	60	80	*	5	70	135	*	4	84	110	*	3	59	91	*	3	83	73		6	78	80	*	15	64	26	
200					3	30	116	***	3	30	70	**	3	41	210	***	3	47	74	*	2	40	162	***	2	58	171	**	3	39	117	**	7	30	39	*
250					2	22	85	***	2	20	50	**	2	25	134	***	2	26	26		1	19	188	***	2	69	193	**	2	26	92	***	5	21	33	*
300	1	83	651	***	1	11	59	***	2	20	50	**	1	14	106	***	2	42	188	***					2	43	180	***	2	26	113	***	3	13	28	**
350					1	11	48	***	1	10	40	***	1	11	16	*	2	90	29		2	39	273	***	1	91	457	***	1	13	74	***	2	09	09	
400					1	11	56	***	2	20	50	**	1	11	16	*	2	27	194	***					1	21	177	***	1	13	43	***	1	04	17	***
450					1	11	41	***																					1	13	44	***	2	08	49	***
500									1	10	120	***	1	11	63	***	1	13	173	***	2	39	108	**	1	48	121	**	1	13	05		1	04	08	*
600					2	22	61	**	1	10	60	***	1	18	106	***	1	13	181	***					2	43	331	***	1	13	67	***	1	04	14	***
700													1	11	28	**													1	13	19	*	1	04	81	***
800					1	11	18	*	2	20	230	***					2	27	482	***													1	04	32	***
900					1	11	58	***																					1	13	131	***	1	04	100	***
1000													1	11	13	*					3	59	302	***					1	13	66	***				
1500									1	10	220	***	1	18	67	***	1	13	105	***					2	43	66	*					2	08	78	***
2000					3	33	130	***	1	10	240	***	1	11	27	**	1	13	94	***									2	26	278	***				
2500																																	1	04	09	**
3000																																				
3500																																				
4000																																				
4500																																	2	08	593	***
5000																																				
>5000																																				

Table 9 (continued)

Set No	28				29				30				31				32				Mean						
Range of W L (km)	N	E	O	S	N	E	O	S	N	E	O	S	N	E	O	S	N	E	O	S	N	E	σ_E	O	σ_S	σ/E	
0	55	649	232		103	620	70	***	21	691	206		80	632	179		54	659	205		62	639	66	187	78	03	
50	15	176	171		34	190	50		9	246	218		24	187	128		14	172	100		19	194	16	134	51	07	
100	5	59	77		13	70	100		3	92	74		8	63	64		5	59	85	*	6	69	13	100	50	14	
150	3	43	0	64	*	6	30	30		2	49	117	**	4	31	45	*	2	26	42	*	3	35	07	84	40	24	
200	2	24	16			4	30	30		2	85	213	**	2	16	27	*	2	24	71	**	3	26	10	82	38	32	
250	2	24	32	*		3	10	50	***	2	52	132	**	2	15	46	***	2	25	187	***	2	25	12	103	93	41	
300	1	12	60	***		2	10	10						1	08	31	***	1	13	39	***	2	21	10	89	60	42	
350	2	24	103	***		2	10	20	**	2	47	192	***	1	08	65	***	1	12	56	***	2	21	06	107	62	51	
400						1	05	10	**													2	13	03	58	27	45	
450	1	12	142	***		1	05	20	***					2	16	275	***	2	24	298	***	2	18	05	125	68	69	
500	1	12	35	**		2	10	130	***	2	52	294	***	1	08	38	***					4	45	07	255	67	57	
600						1	05	40	***									1	13	06		4	32	05	205	51	64	
700	2	24	90	***		2	10	170	***					1	08	58	***	1	12	56	***	4	41	05	338	90	82	
800						1	05	60	***													4	25	02	250	41	100	
900																						4	39	06	287	72	74	
1000	1	12	474	***		3	20	140	***	2	47	638	***	2	16	86	***					16	157	05	1440	80	92	
1500	2	23	309	***														3	37	485	***	13	129	01	1728	95	134	
2000						1	05	240	***					2	16	455	***					13	90	01	2195	138	244	
2500																						4	19	0	357	44	188	
3000						1	10	250	***													1	07	0	251	0	354	
3500																						1	05	0	27	0	50	
4000						1	05	250	***													3	13	0	842	182	648	
4500																						5	21	0	232	12	110	
5000																						2	08	0	314	87	392	
> 5000																												

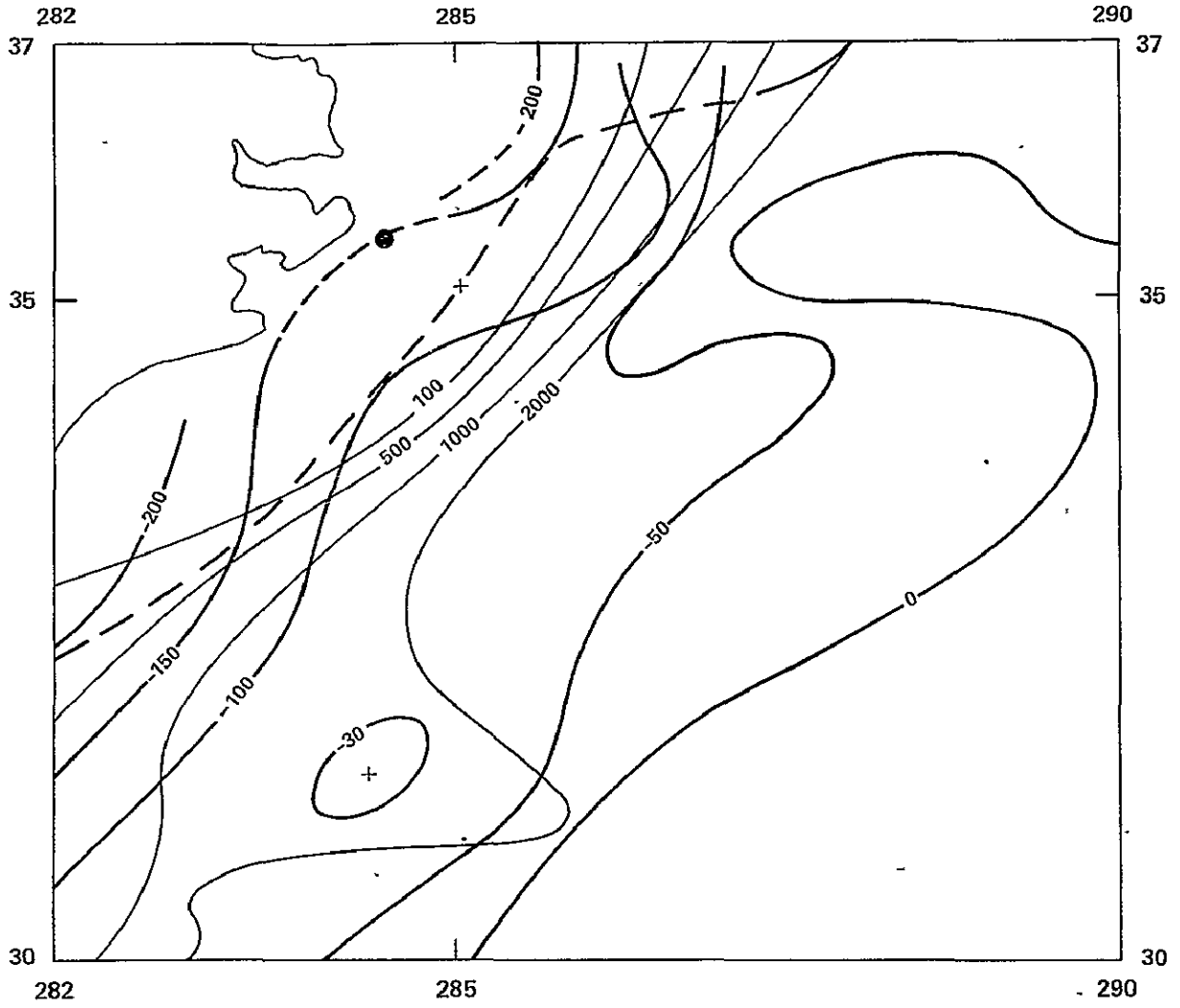

Figure A1. Smoothed Guestimates of Quasi-Stationary Sea Surface Topography in the Vicinity of the Gulf Stream–Epoch: – July 1975 – August 1976

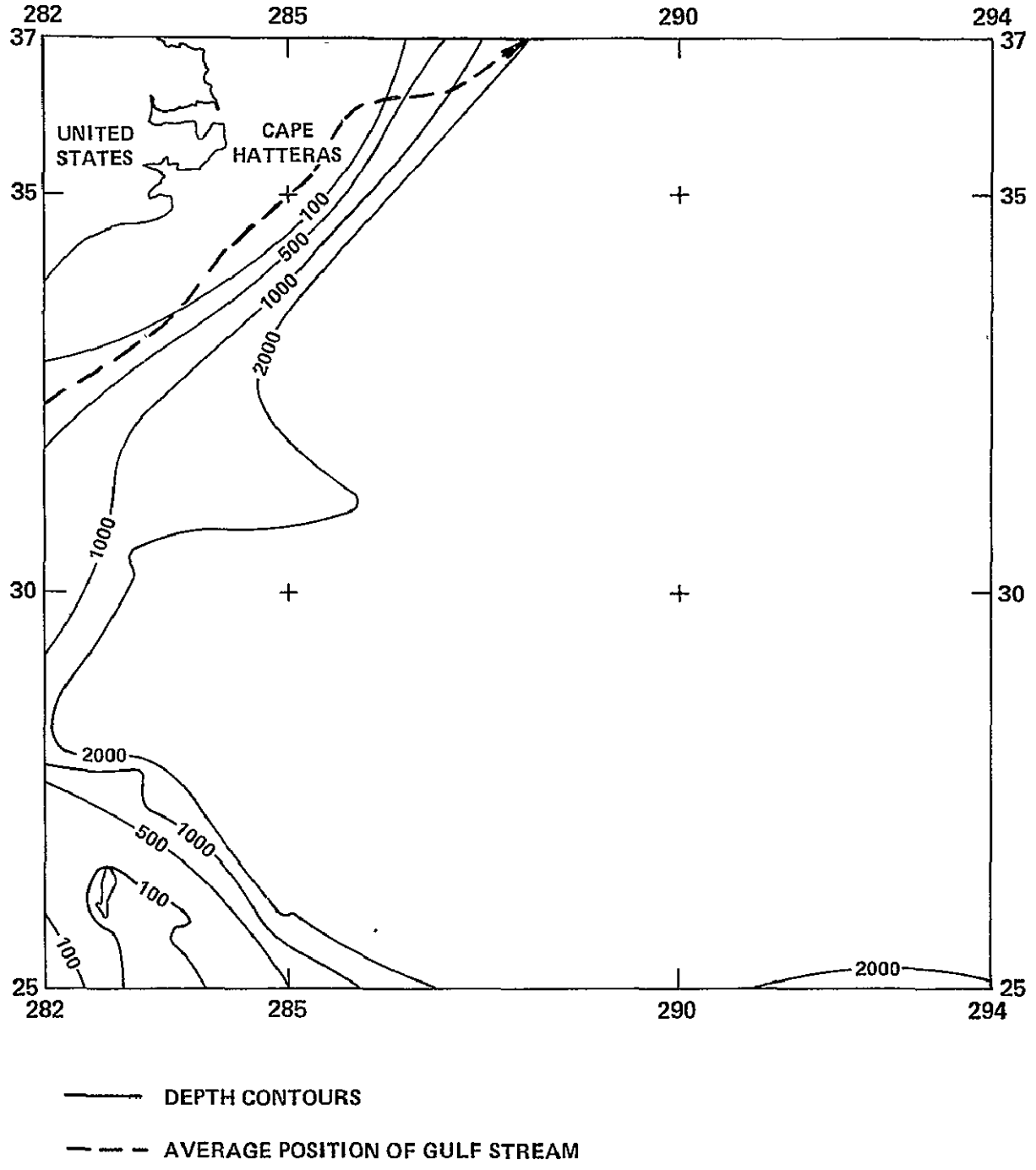

Figure 1. The Sargasso Sea Test Area

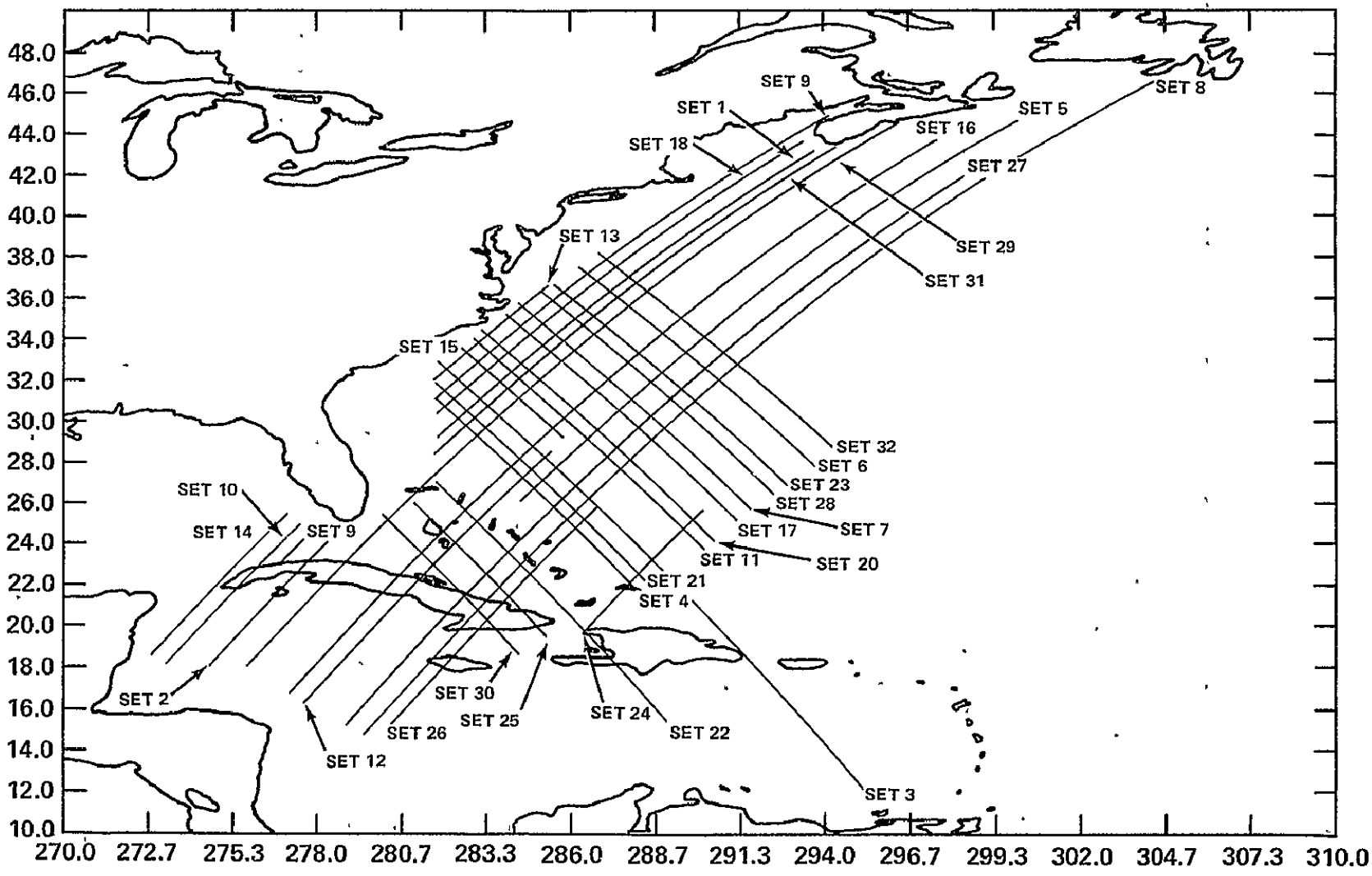

Figure 2. Sets of Overlapping Passes of GEOS-3 Altimetry in the Western North Atlantic

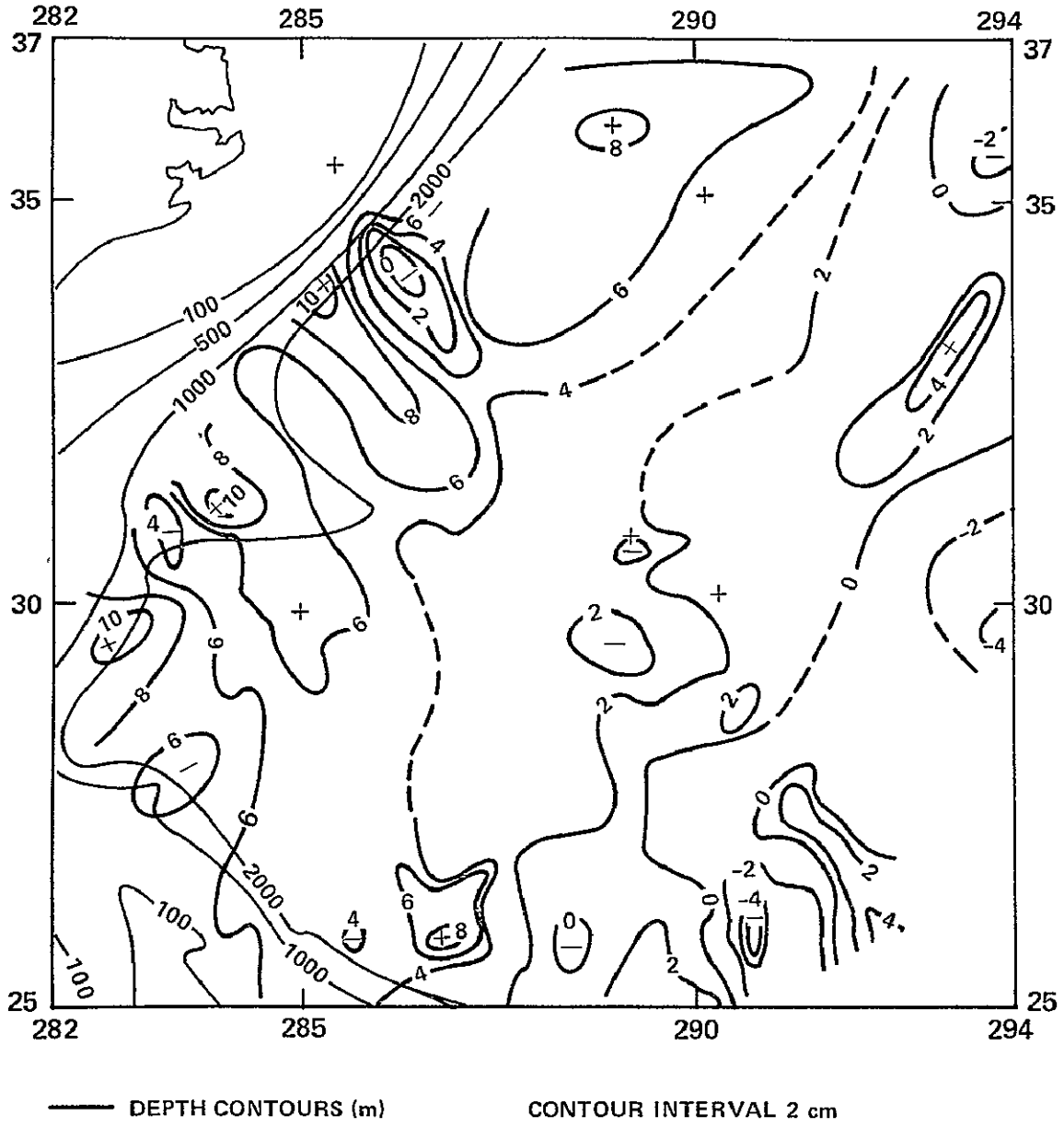

Figure 3. Sea Surface Models of Sargasso Sea –
October 1975 Differences [Tide Corrected Model – Uncorrected Model]

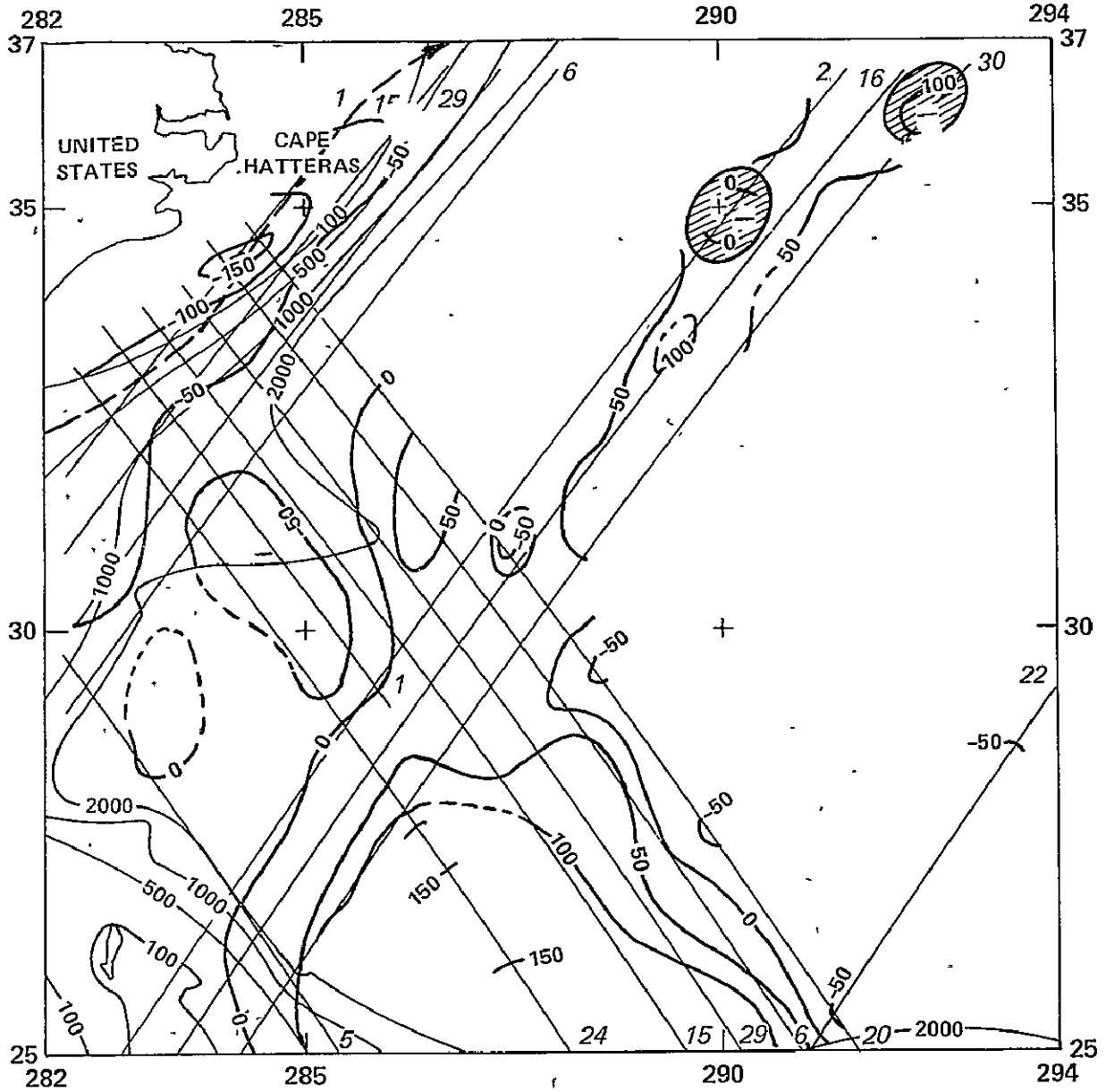

Figure 4. Regional Model of Dynamic Sea Surface Topography Variations – Sargasso Sea – July 1975

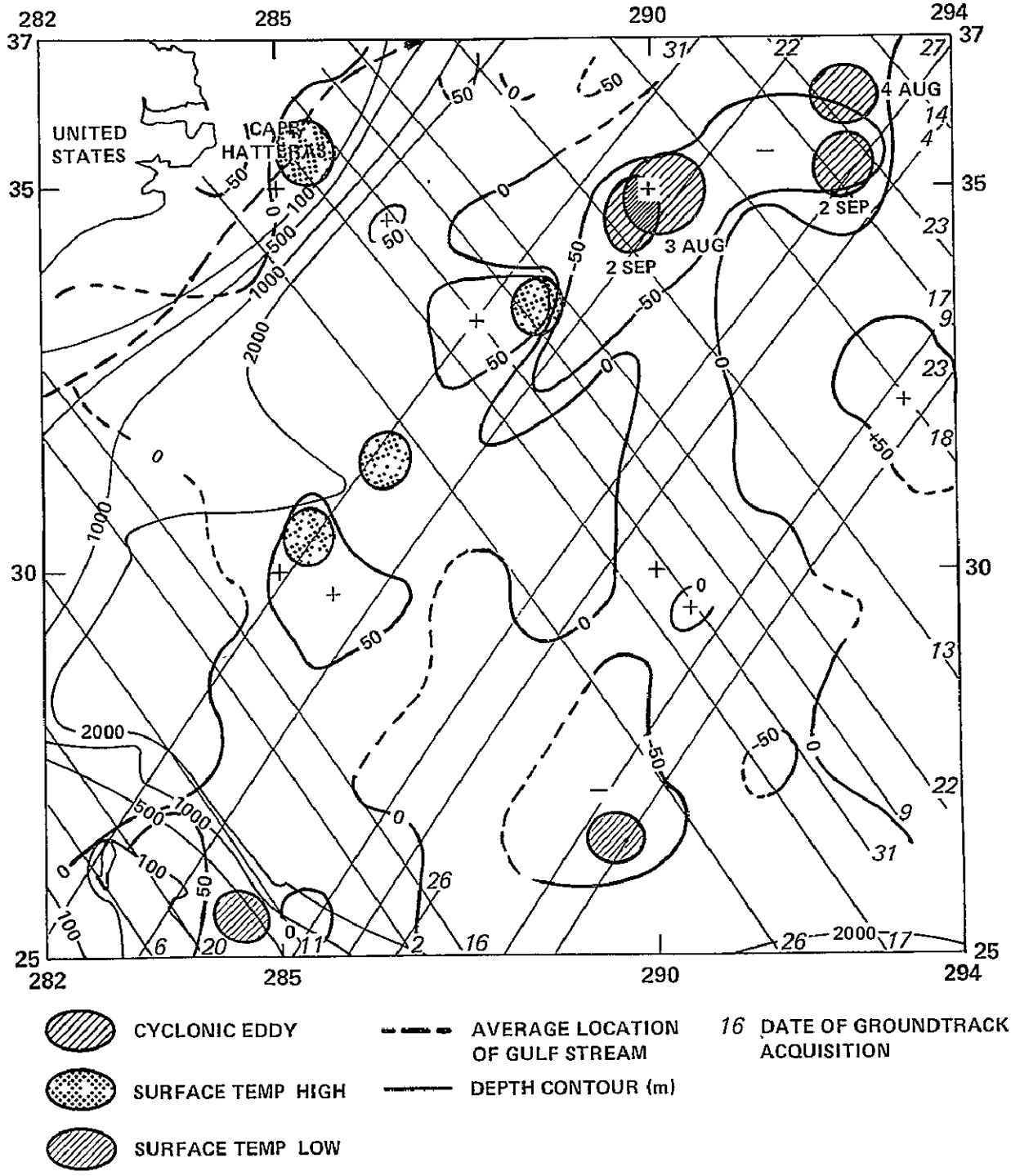

Figure 5. Regional Model of Dynamic Sea Surface Topography Variations – Sargasso Sea – August 1975

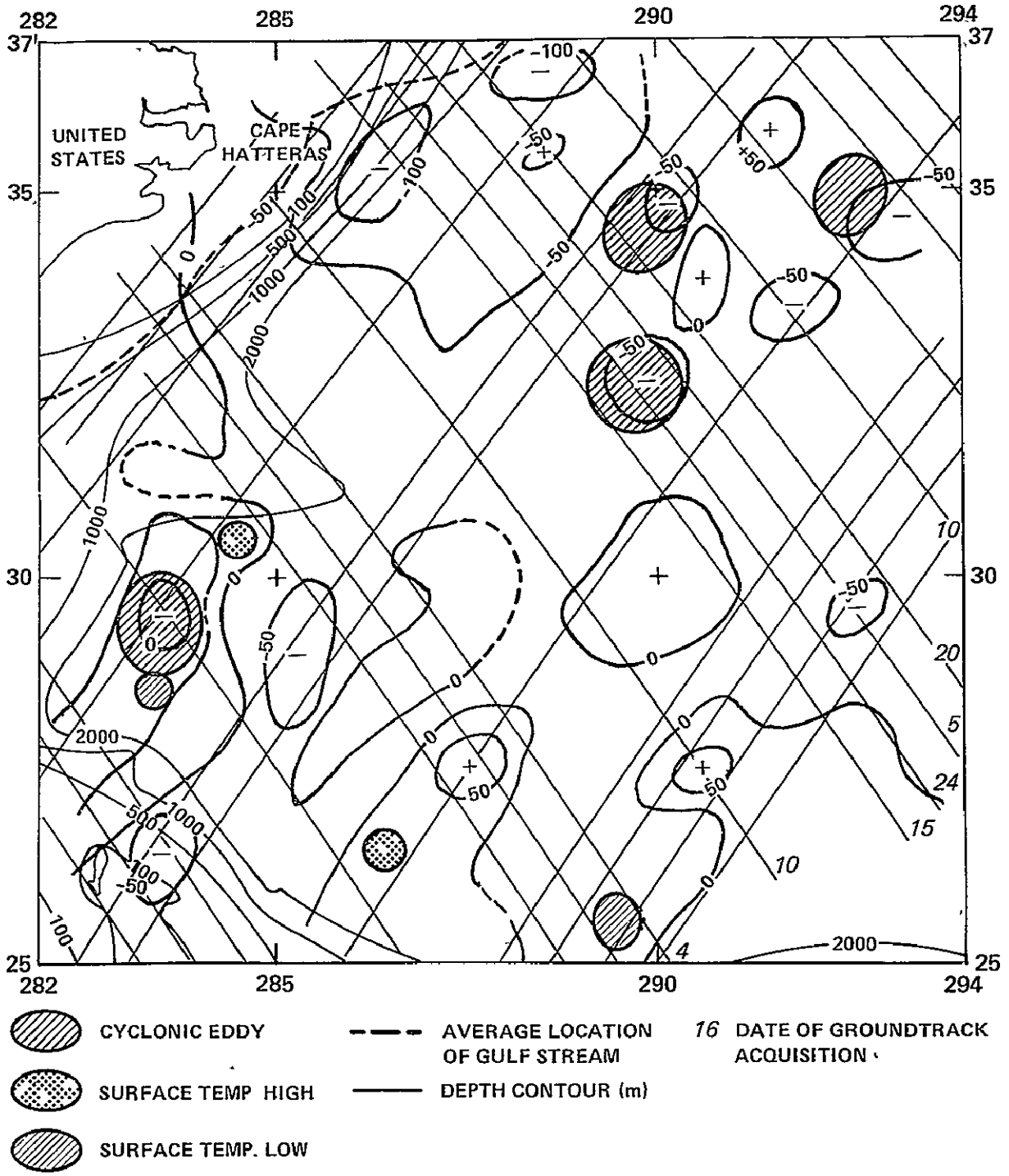

Figure 6. Regional Model of Dynamic Sea Surface Topography Variations – Sargasso Sea – September 1975

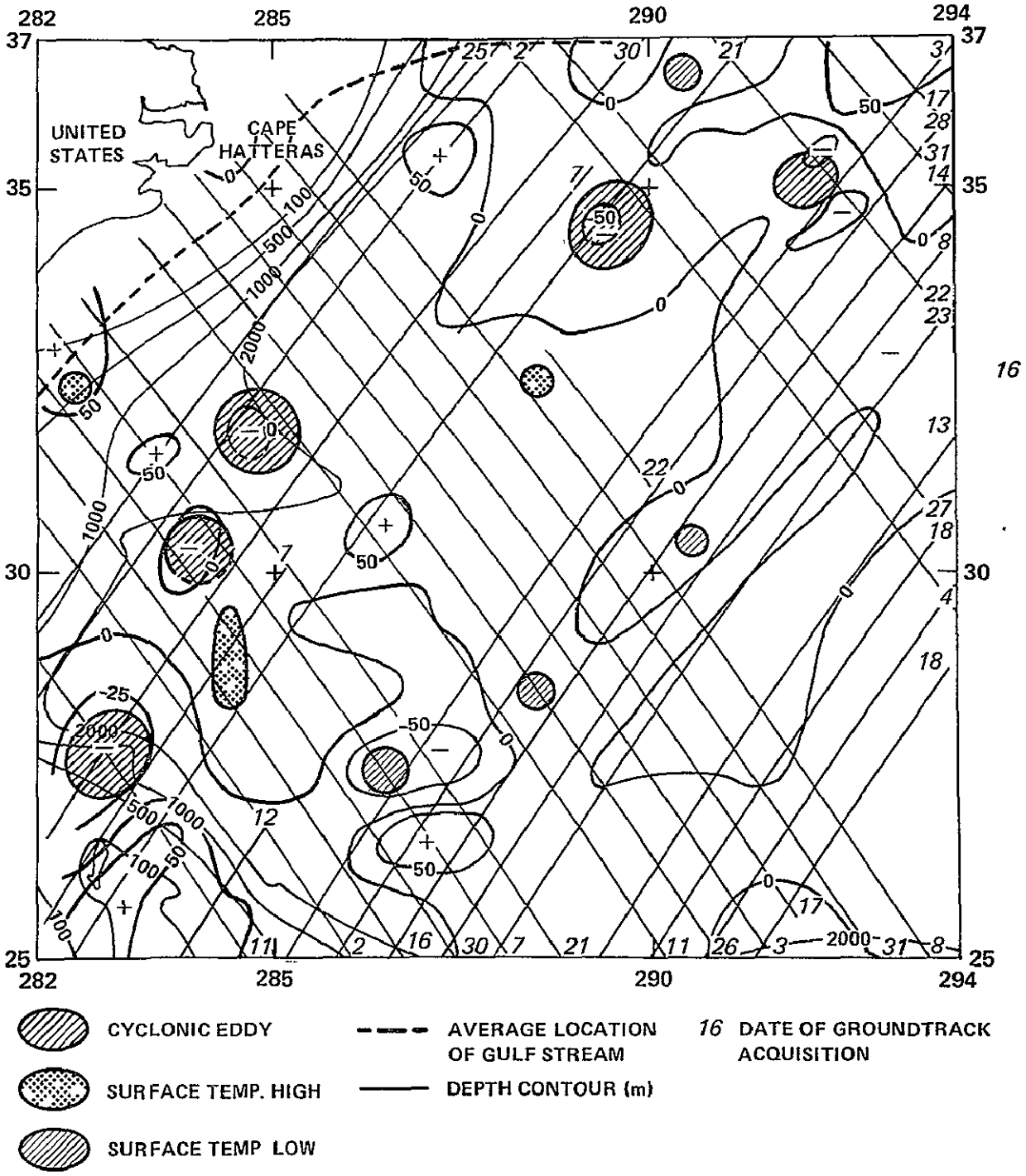

Figure 7. Regional Model of Dynamic Sea Surface Topography Variations – Sargasso Sea – October 1975

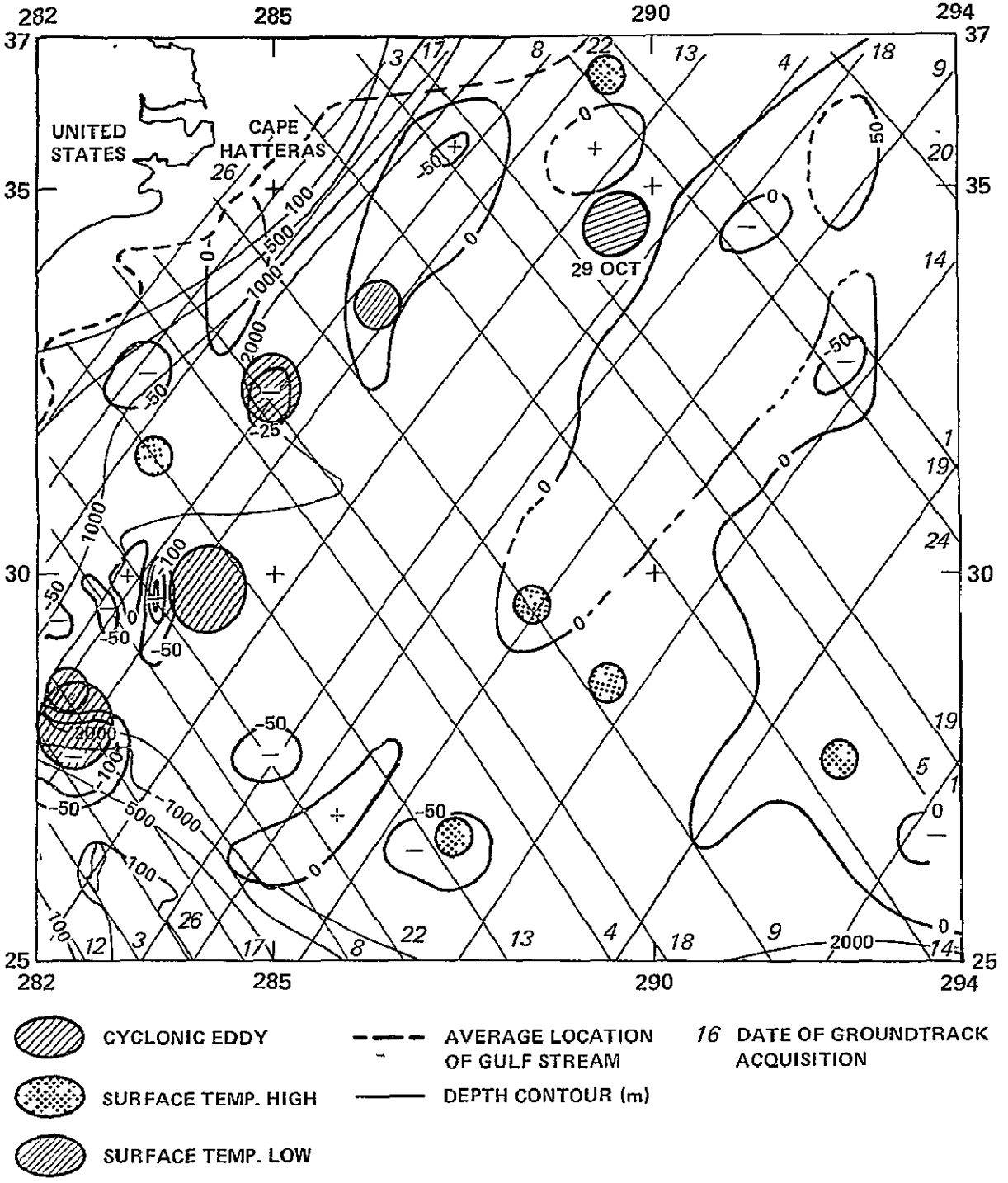

Figure 8. Regional Model of Dynamic Sea Surface Topography Variations – Sargasso Sea – November 1975

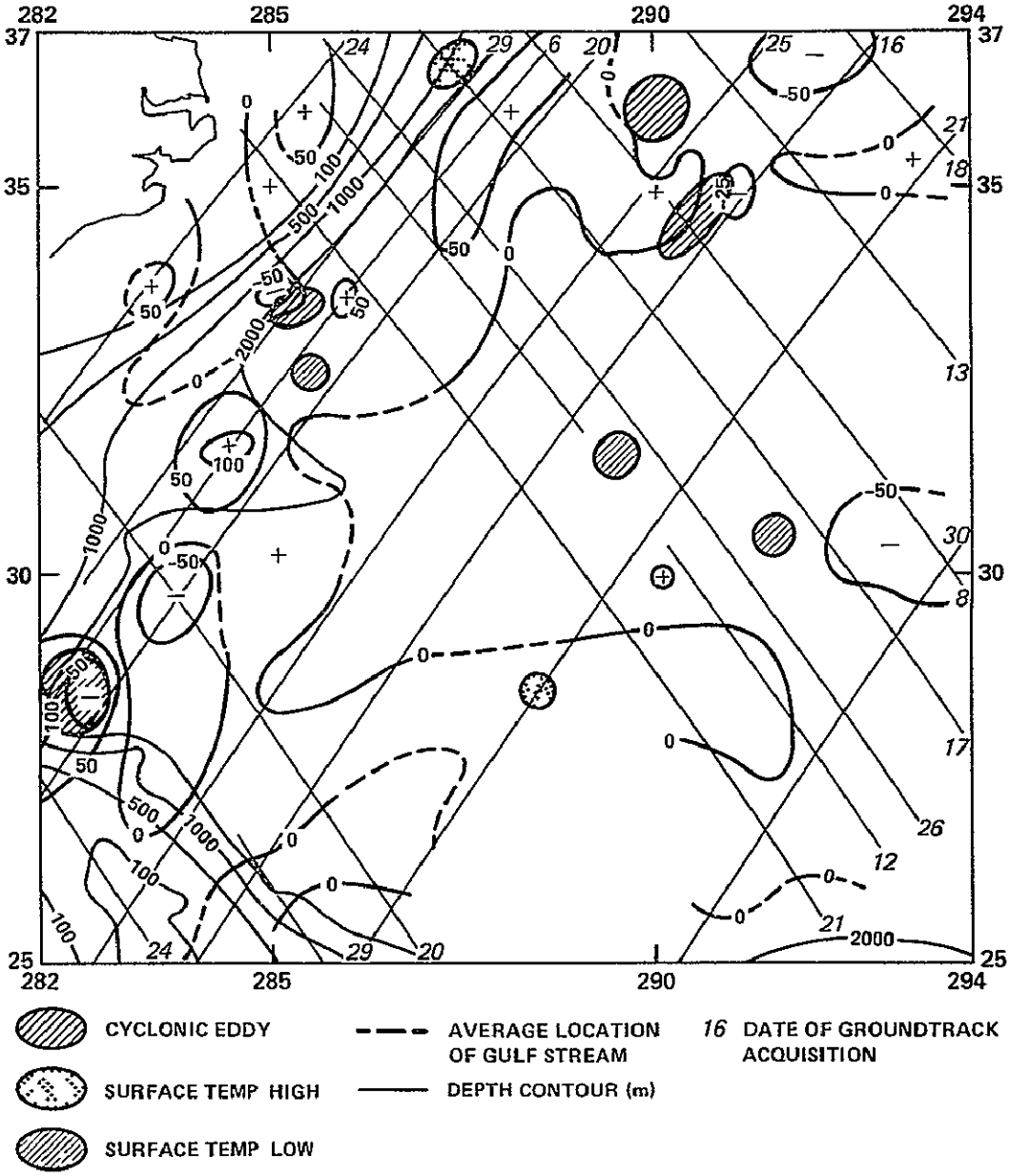

Figure 9. Regional Model of Dynamic Sea Surface Topography Variations – Sargasso Sea – April 1976

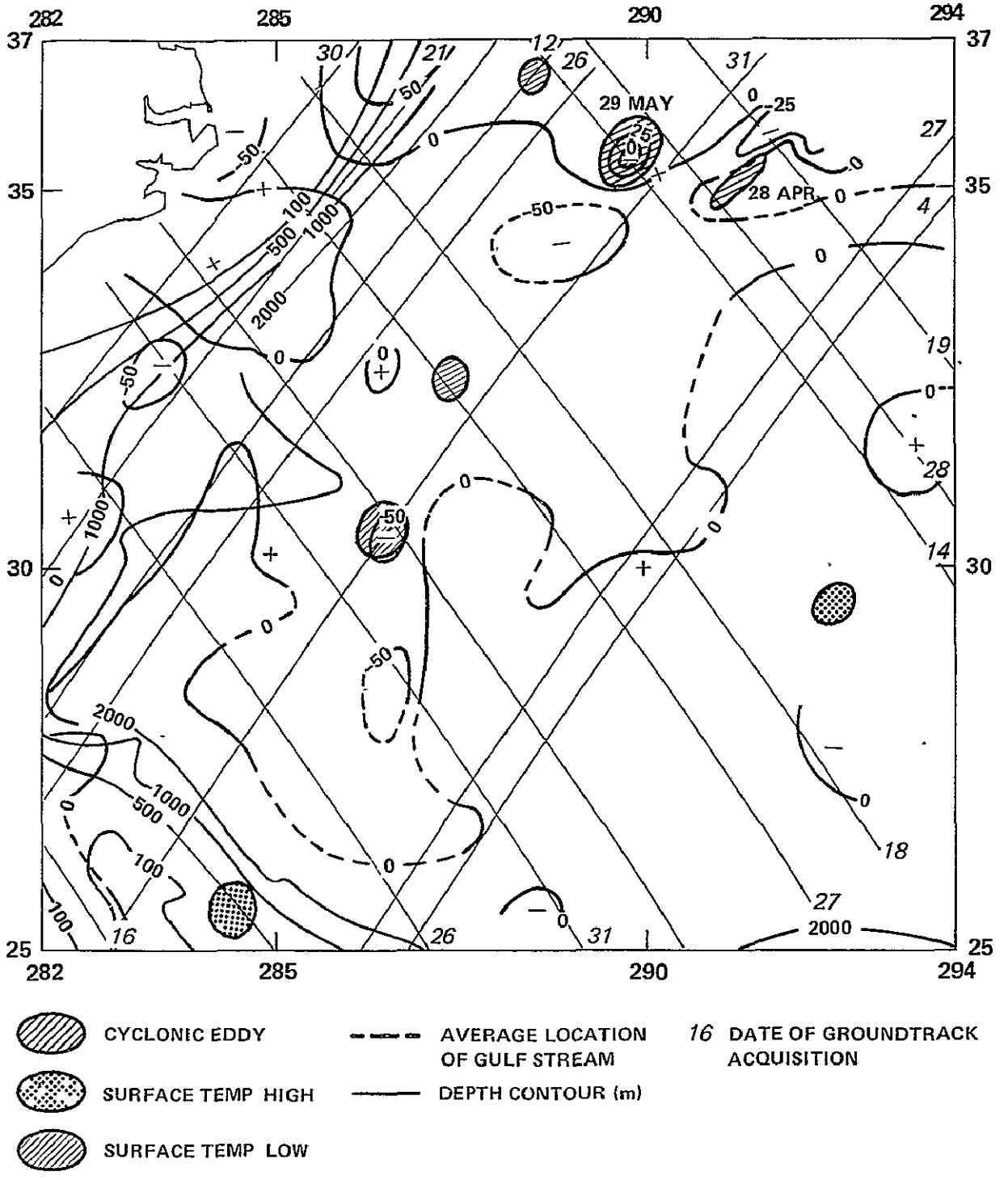

Figure 10. Regional Model of Dynamic Sea Surface Topography Variations – Sargasso Sea – May 1976

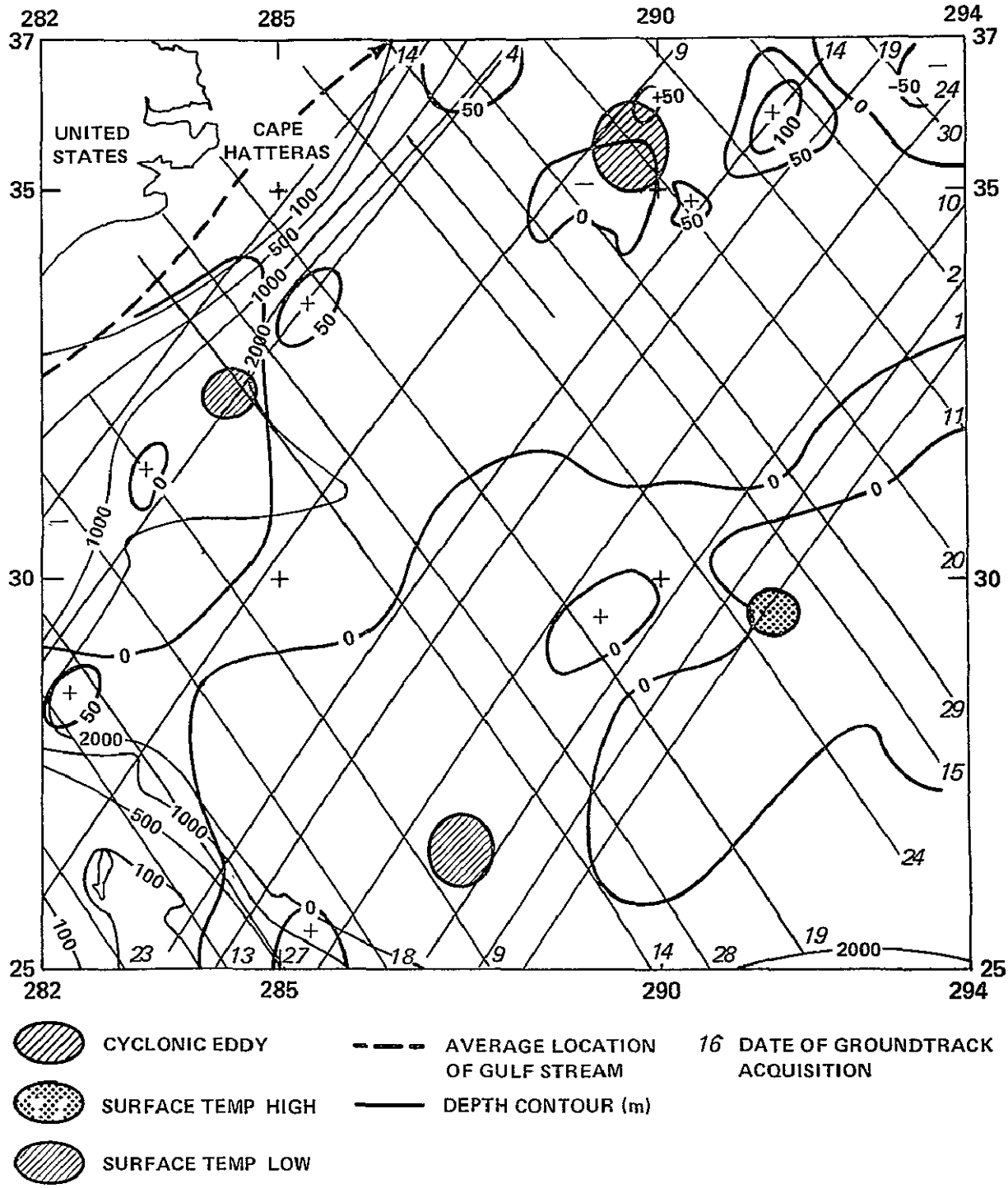

Figure 11. Regional Model of Dynamic Sea Surface Topography Variations – Sargasso Sea – June 1976

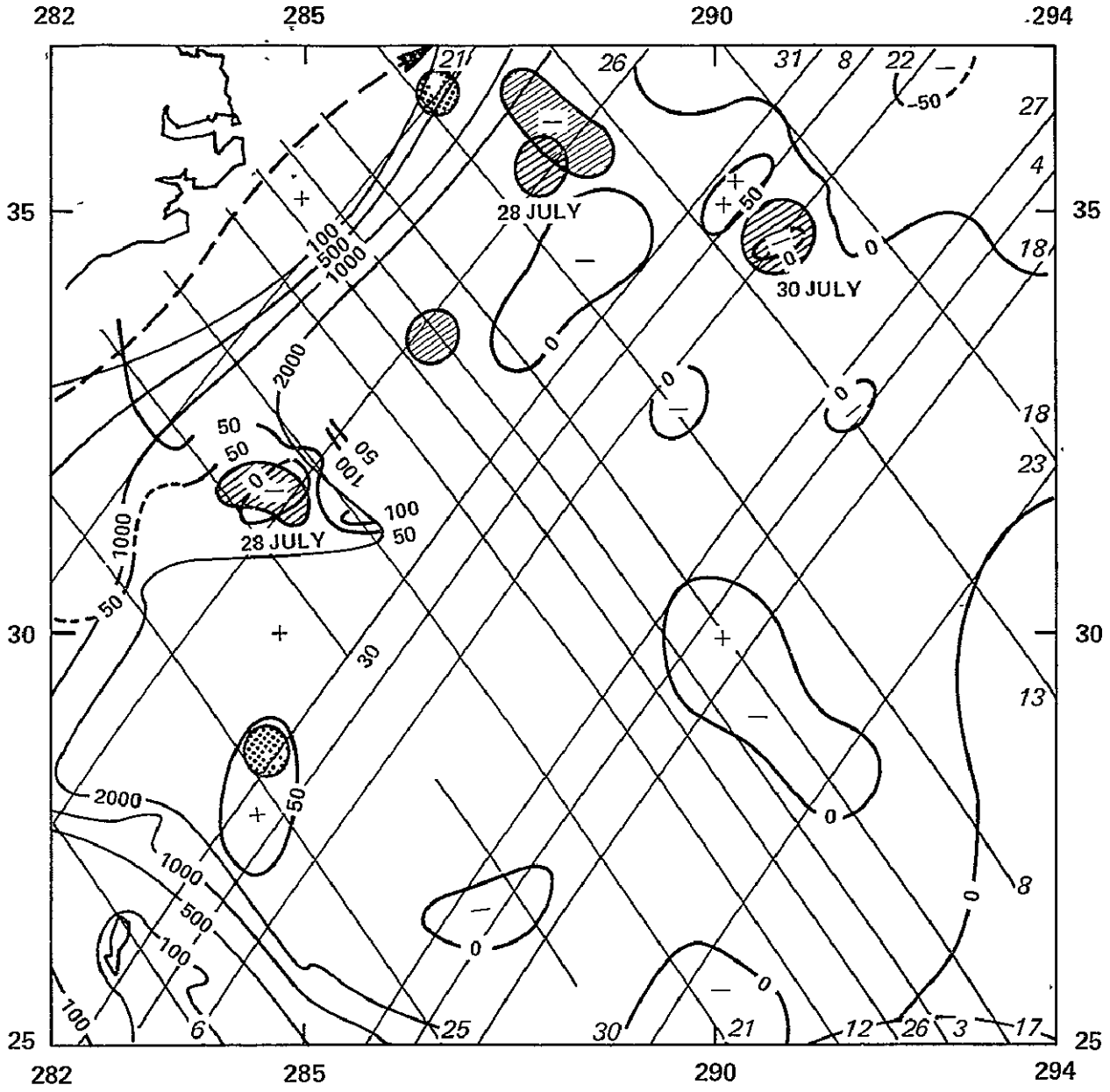

DATUM – AVERAGE SEA SURFACE FOR JULY 1975 – AUGUST 1976

CONTOUR INTERVAL 50 cm WAVELENGTHS >200 km

Figure 12. Regional Model of Dynamic Sea Surface Topography Variations – Sargasso Sea – July 1976

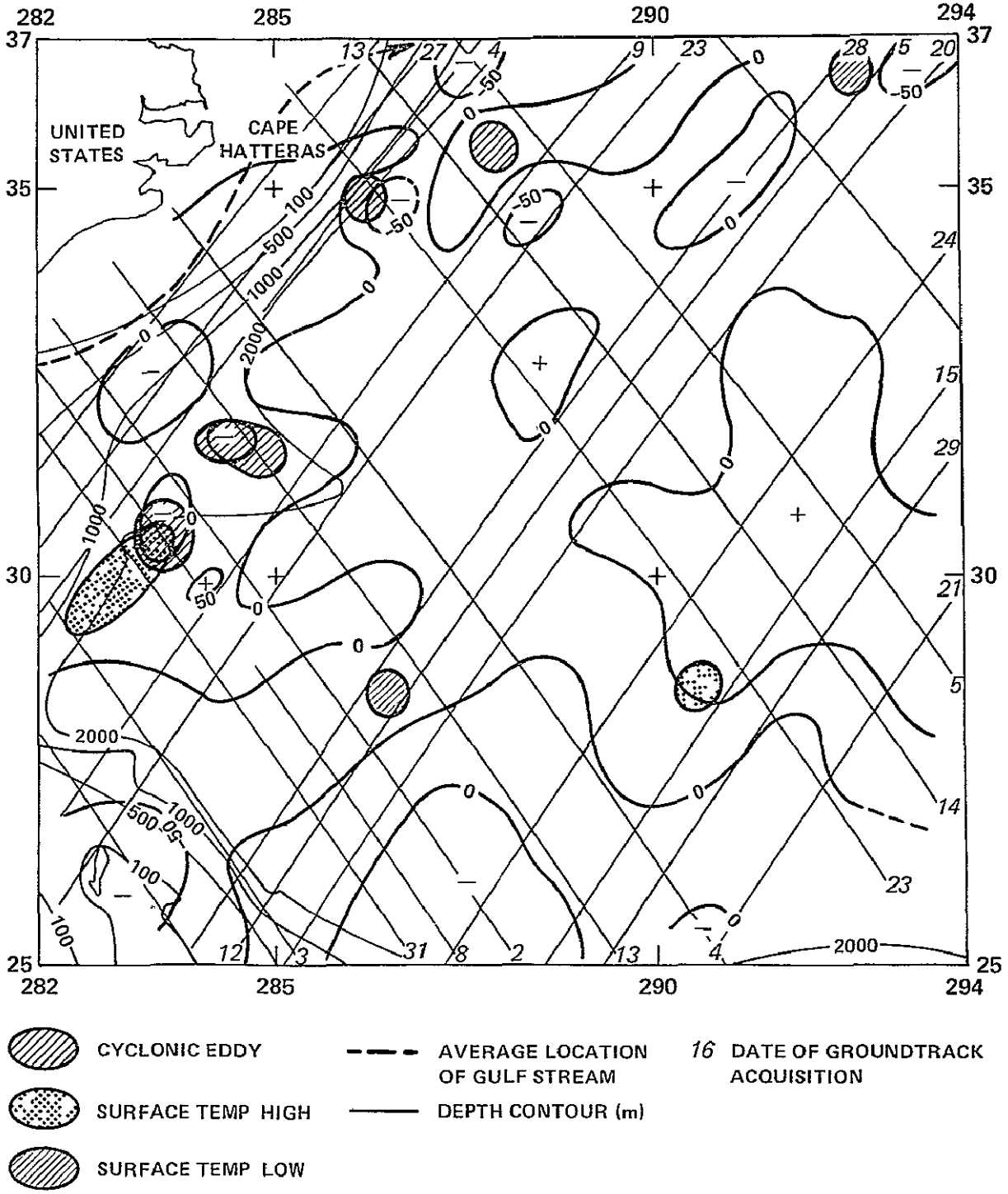

Figure 13. Regional Model of Dynamic Sea Surface Topography Variations – Sargasso Sea – August 1976

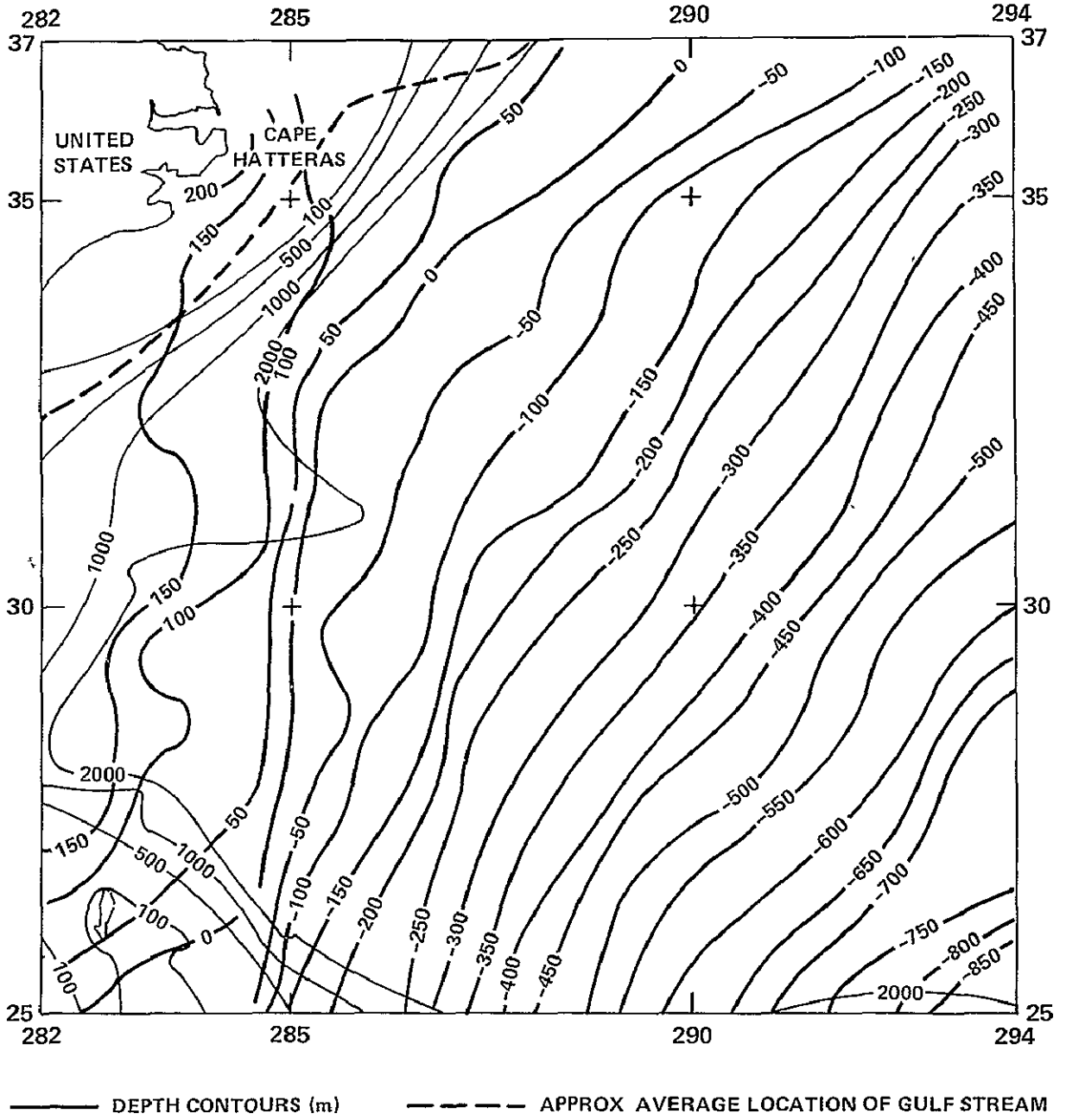

Figure 14. Sargasso Sea Discrepancies Between Average Sea Surface (Oriented on GEM 9) and Marsh 5 Minute Gravimetric Geoid. Contour Interval – 50 cm

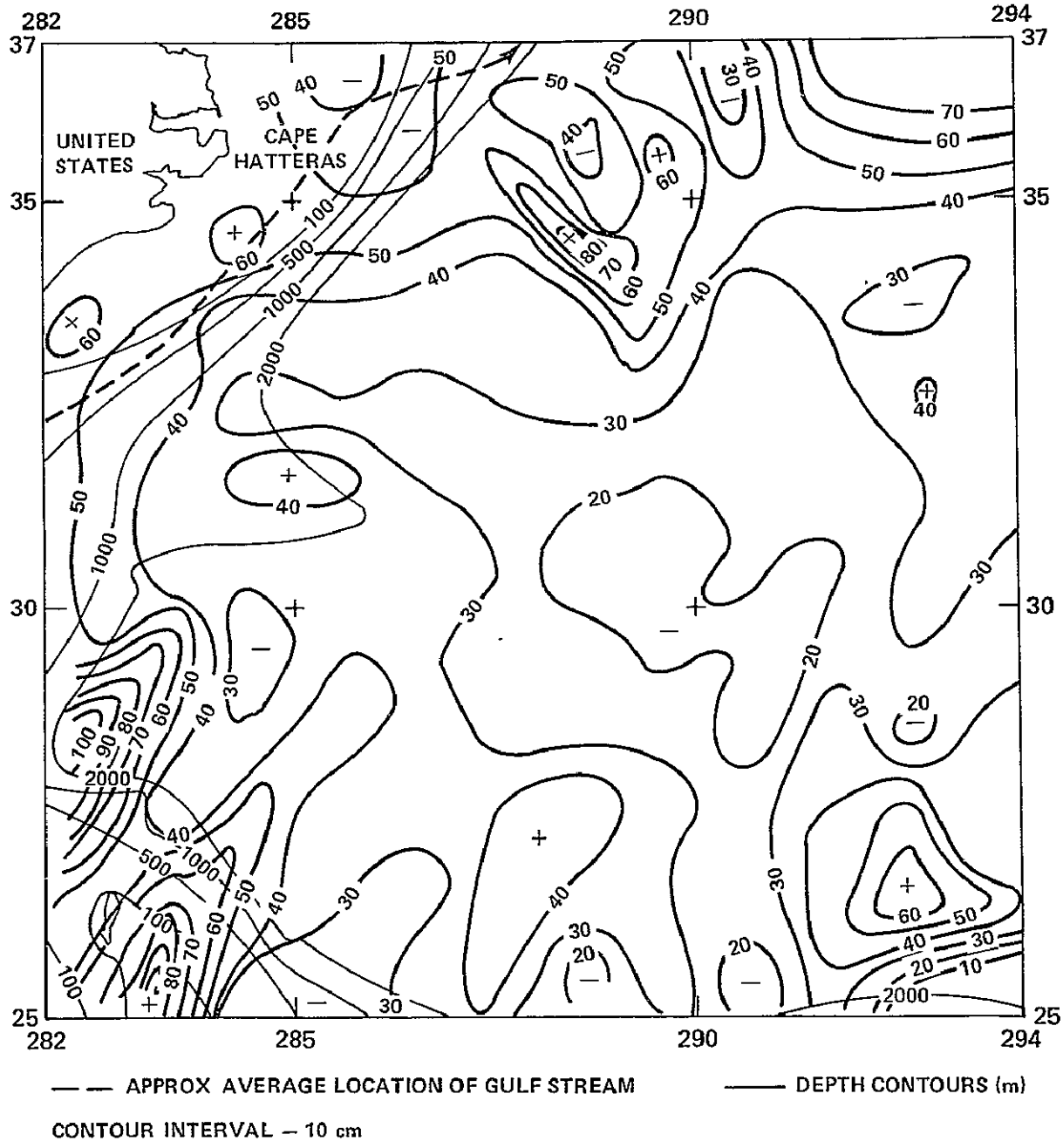

Figure 15. Sargasso Sea Variation of Monthly Sea Surface Heights as a Function of Position (rms residual ± cm)

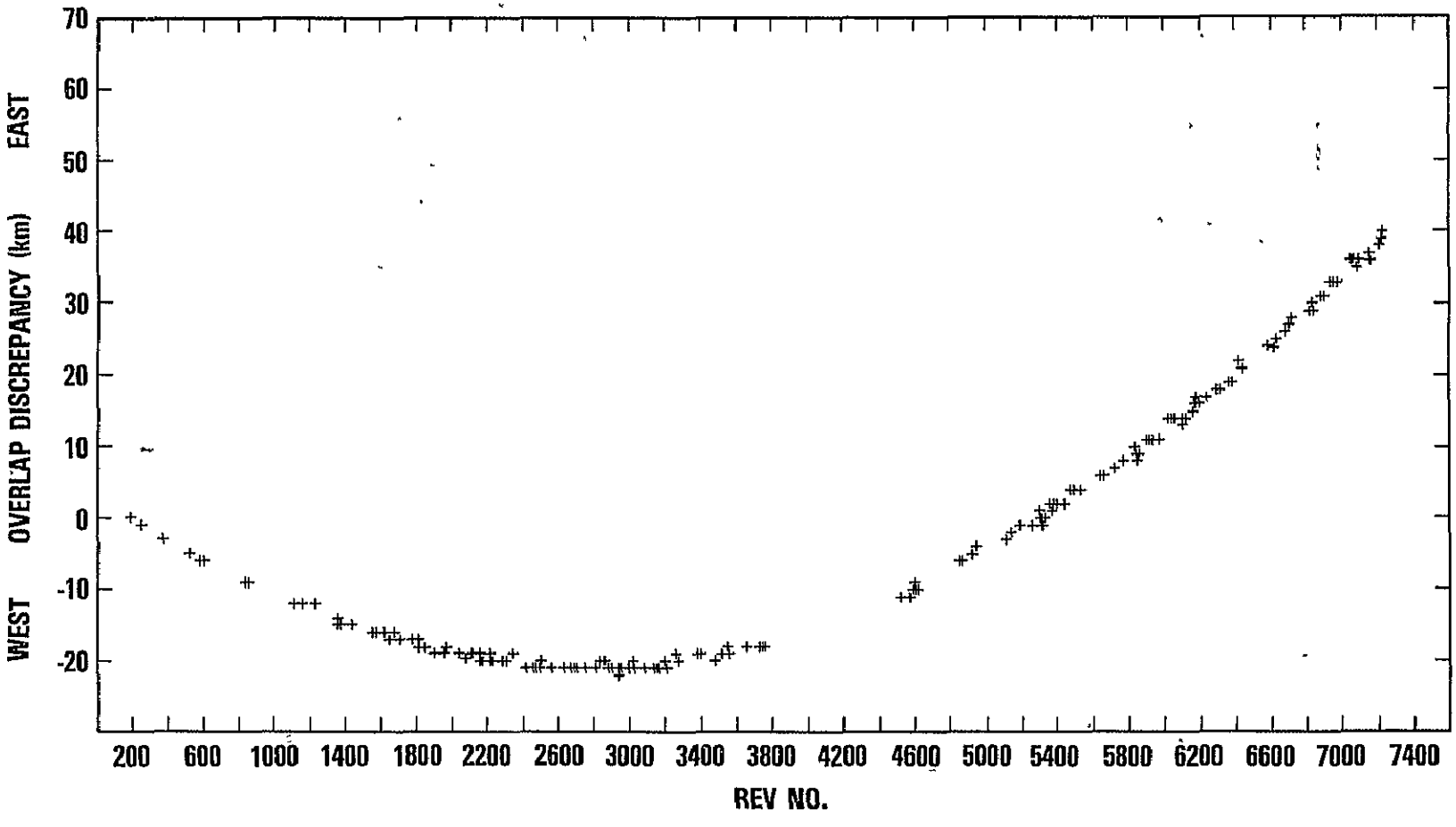

Figure 16. Offset in Longitude for Overlapping Passes as a Function of Time

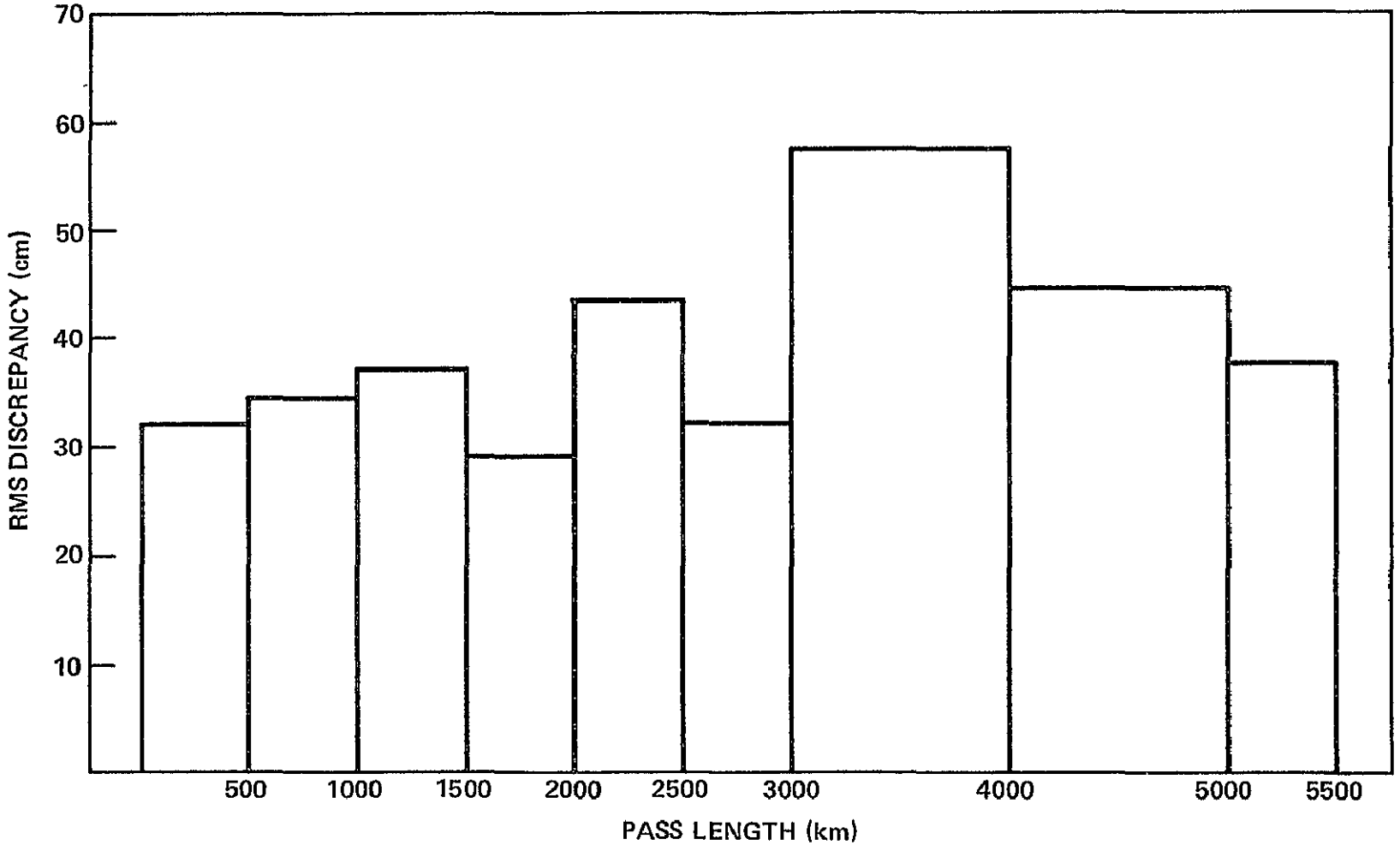

Figure 17. Root Mean Square (RMS) Discrepancy as a Function of Pass Length

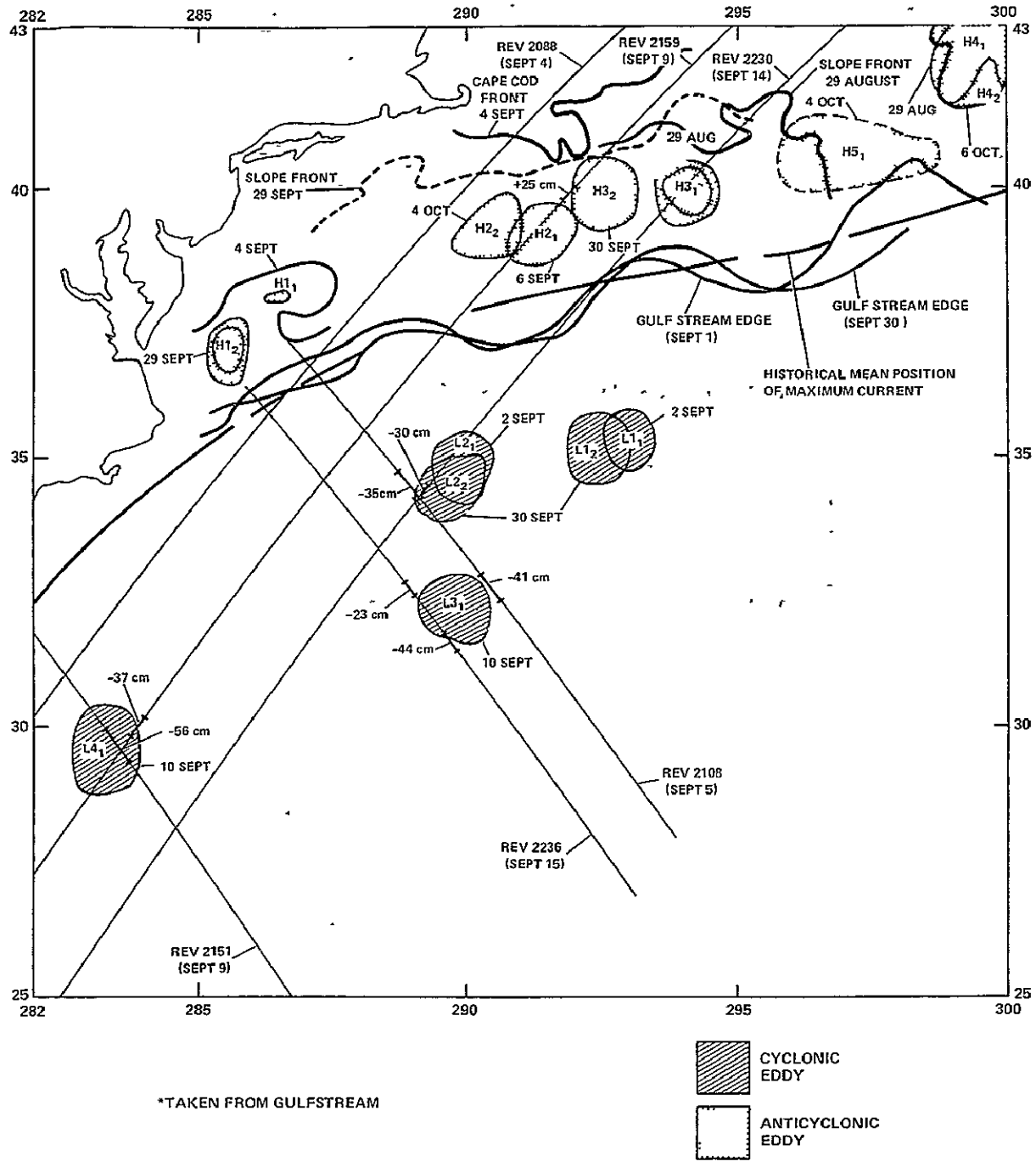

Figure 18. Correlation of Infra-red Imagery with GEOS-3 Altimetry Profiles (September 1975)*

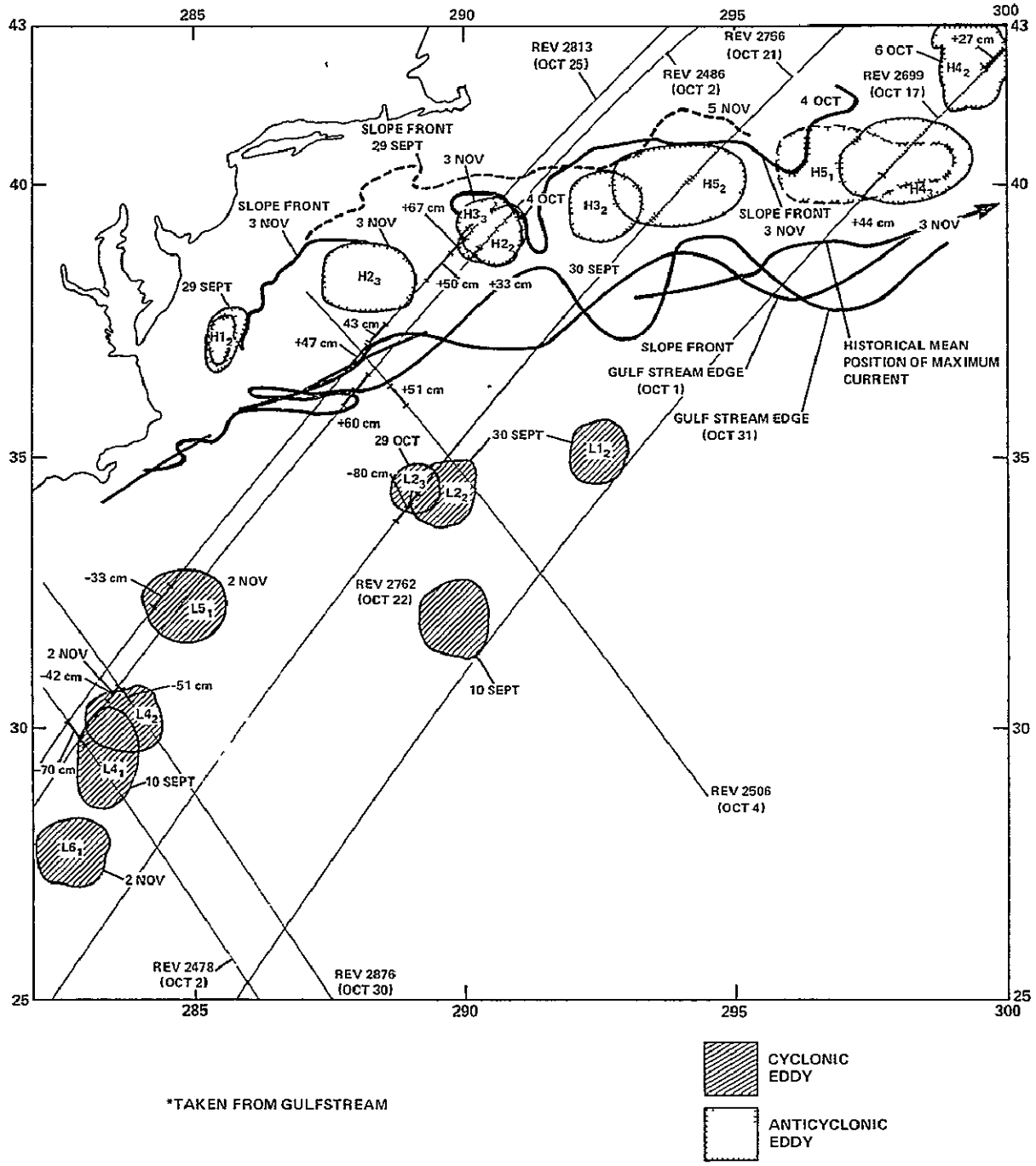

Figure 19. Correlation of Infra-red Imagery with GEOS-3 Altimetry Profiles (October, 1975)*

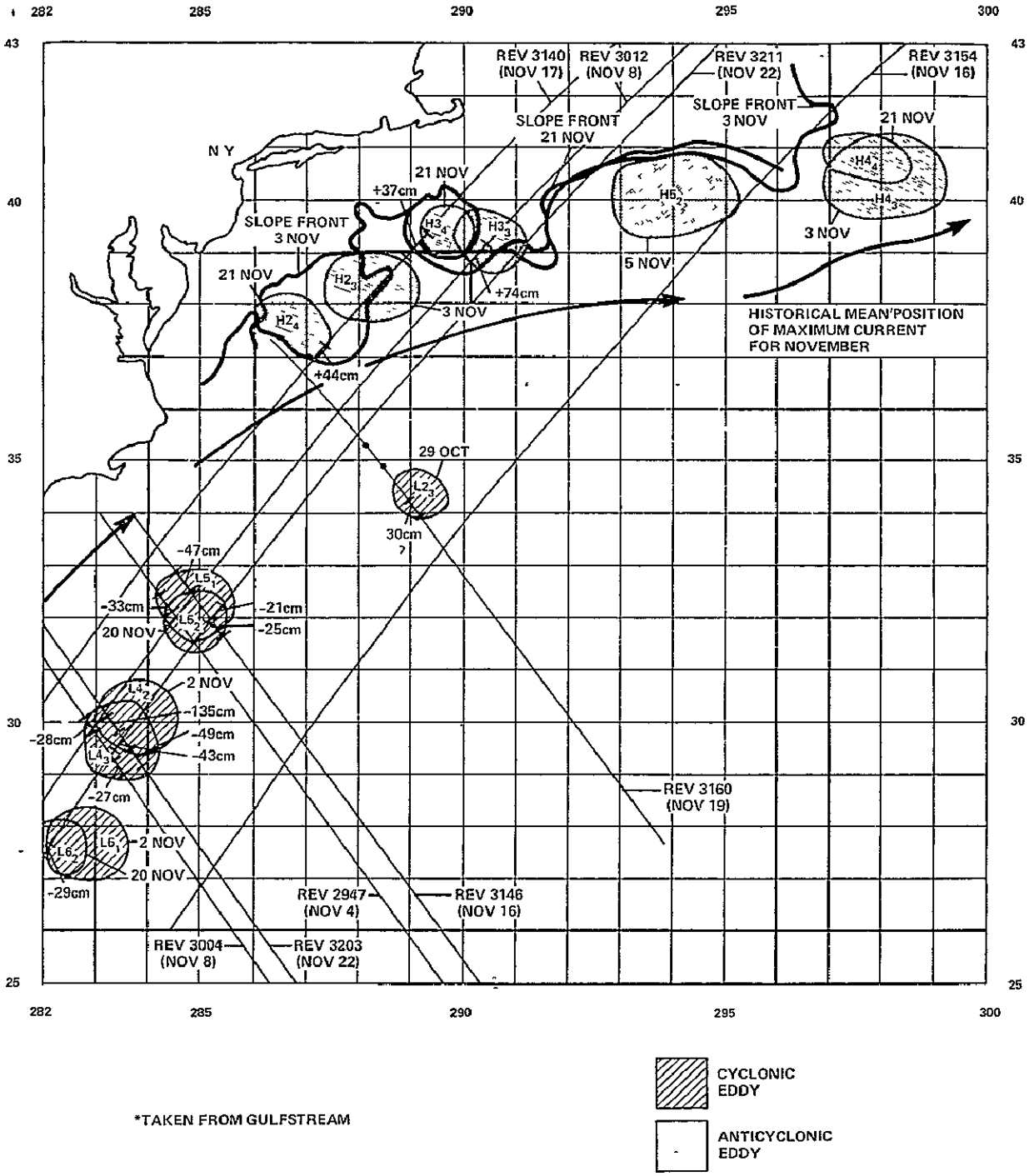

Figure 20. Correlation of Infra-red Imagery with GEOS-3 Altimetry Profiles (November 1975)*

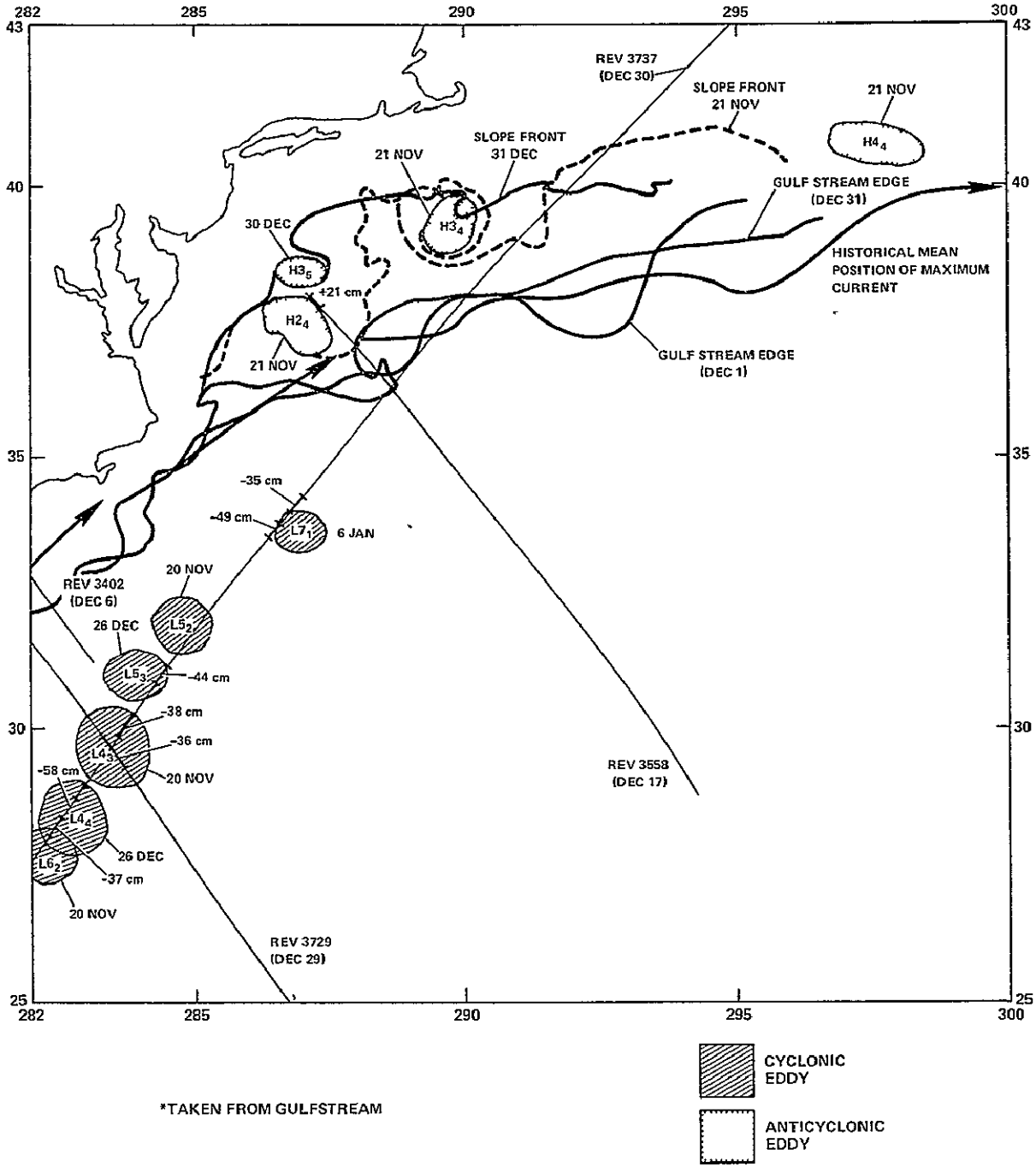

Figure 21. Correlation of Infra-red Imagery with GEOS-3 Altimetry Profiles (December 1975)*

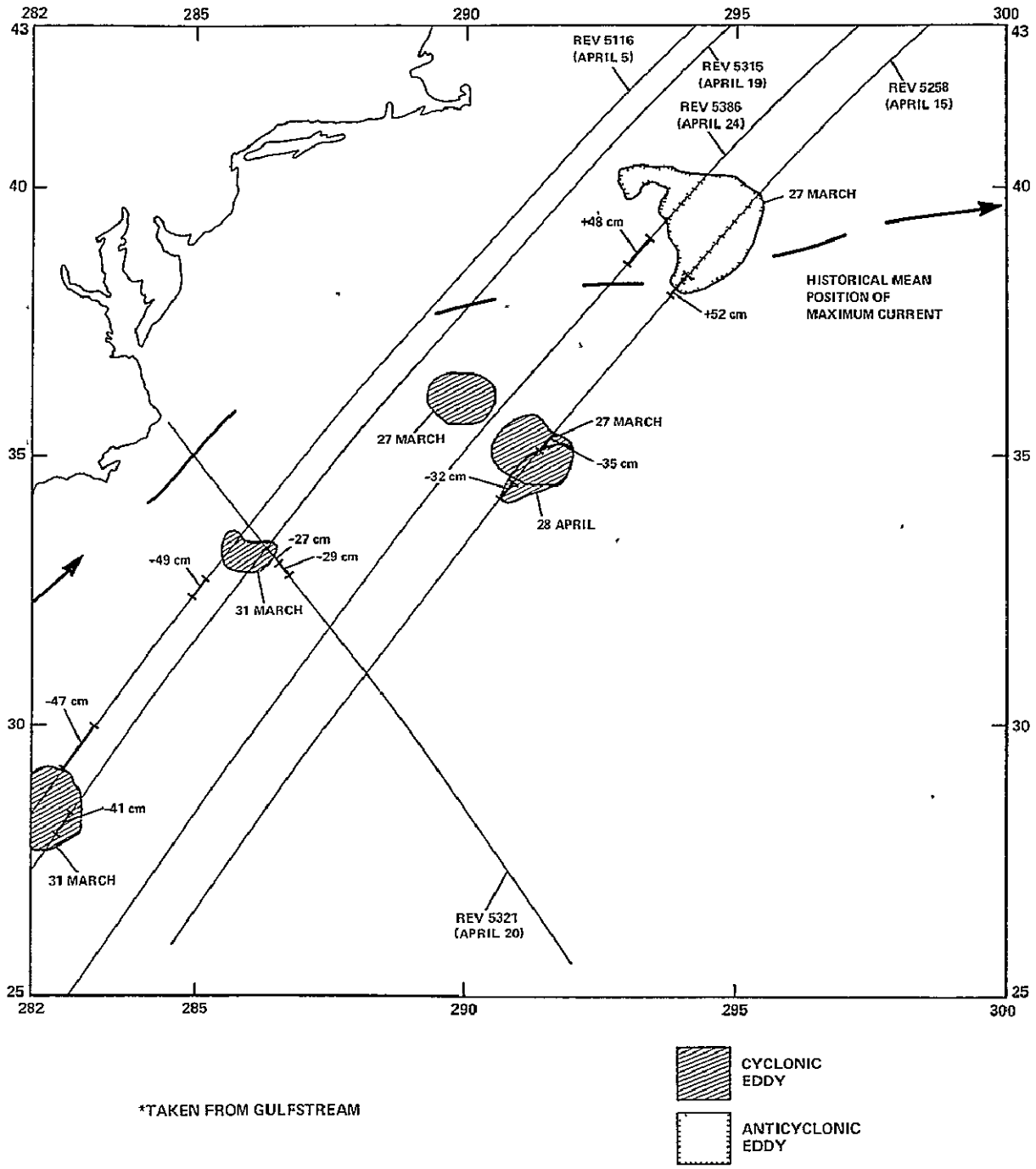

Figure 22 Correlation of Infra-red Imagery with GEOS-3 Altimetry Profiles (April 1976)*

BIBLIOGRAPHIC DATA SHEET

1 Report No.	2. Government Accession No.	3. Recipient's Catalog No
TM 79549		

4. Title and Subtitle	5 Report Date
The Analysis of Temporal Variations in Regional Models of the Sargasso Sea from GEOS-3 Altimetry	May 1978
	6. Performing Organization Code
7. Author(s)	8. Performing Organization Report No.
R.S. Mather, R. Coleman and B. Hirsch	921
9. Performing Organization Name and Address	10. Work Unit No.
Goddard Space Flight Center Geodynamics Branch, Code 921 Greenbelt, MD 20771	11. Contract or Grant No. NSG 5225
	13. Type of Report and Period Covered Technical Memorandum July 1975 to August 1976
12. Sponsoring Agency Name and Address	14 Sponsoring Agency Code
Same as above	

15 Supplementary Notes

16 Abstract

Monthly regional models of the Sargasso Sea in the western North Atlantic are produced for the periods July to November 1975 and April to August 1976 from GEOS-3 altimetry. The average variability of the models over the period is ± 43 cm. 25% of this value is due to modeling procedures used in the study. Another non-oceanographic contribution comes from instabilities introduced by variable pass geometry. Shortwave maxima and minima in the regional sea surface models are examined for correlations with surface and remote sensed infrared temperature data. On allowing for differences in the quantities being compared, an 88% correlation is obtained on comparison with cyclonic eddies reported by the National Weather Service. This figure drops to 59% in the case of correlations with maxima and minima of surface temperature fields.

The analysis of 32 sets of 5 to 9 overlapping passes provides a better picture of instantaneous sea state through wavelengths greater than 30 km. The improved resolution (± 33 cm) shows that the variability of the Sargasso Sea through wavelengths between 150 and 5000 km is ± 18 cm.

17. Key Words (Selected by Author(s))	18. Distribution Statement
GEOS-3 Altimetry Sargasso Sea Sea Surface Topography Variations Cyclonic Eddies	

19. Security Classif. (of this report)	20. Security Classif (of this page)	21 No. of Pages	22 Price*

*For sale by the National Technical Information Service, Springfield, Virginia 22151

GSFC 25-44 (10/77)